

## Response to Reviewers' Comments

*We thank both reviewers for their careful reading of the manuscript and for their useful insights. Below, the comments from the reviewers are shown in black. The responses to the comments are shown in blue and the changes to the manuscript are shown in bold blue.*

### **Anonymous Referee #1**

In this work, the authors used a new analytical technique that allows for high time resolution and sensitive measurements of nitrated phenols in the gas phase. The measurement technique is based on time of flight chemical ionization mass spectrometry (ToF-CIMS) with acetate as the reagent ion. The sampling was conducted in winter of 2014 at the Horse Pool site in the Uintah Basin. The authors combined the measured diurnal profile of nitrophenols with box model simulations to provide insight into the generation and removal pathways of the nitrophenols. Overall, this is a nice manuscript that demonstrates the ability of the techniques to measure low level of nitrated VOCs and improve our understanding of their evolution in the atmosphere. The manuscript is recommended for publication. More detailed comments follow below:

**Reply:** We would like to thank the reviewer for these valuable comments.

1. P15, L2 Different vapor pressures for 2,4-dinitrophenol and 4-nitrophenol were reported in the literature (Mackay et al., 2006) with values ca. 2 orders of magnitude lower than in Schwarzenbach et al. (1988), this might explain the difference in the calculated fraction of nitrophenols in the particle phase in this work and the experimental data for 4-NP (Cecinato et al., 2005) and DNP (Morville et al., 2006).

**Reply:** We checked all of the vapor pressure values for 4-nitrophenol and 2,4-dinitrophenol compiled from various literatures sources in Mackay et al. (2006). The differences among the values listed in Mackay et al. (2006) are partially due to the different vapor pressures for solid and sub-cooled liquid at the same temperature. For the ideal gas-particle absorption partitioning theory, vapor pressure of sub-cooled liquid should be used (Yatavelli et al., 2014). The solid vapor pressure  $p_s(T)$  and sub-cooled liquid vapor pressure  $p_L(T)$  at temperature  $T$  are related as (Cappa et al., 2008):

$$\ln \frac{p_L(T)}{p_s(T)} = \frac{\Delta S_{fus}}{R} \left( \frac{T_m}{T} - 1 \right)$$

where,  $\Delta S_{fus}$  is the entropy of fusion (60.1 J/mol\*K for 4-nitrophenol and 62.3 J/mol\*K for 2,4-dinitrophenol from the NIST Chemistry WebBook),  $T_m$  is the melting temperature (385 K for 4-nitrophenol and 388 K for 2,4-dinitrophenol from the NIST Chemistry WebBook), and  $R$  is the gas constant. At 298 K,  $\frac{p_L(T)}{p_s(T)}$  for 4-nitrophenol and 2,4-dinitrophenol are 8.25 and 9.61, respectively. After correcting all of the solid vapor pressures to sub-cooled liquid vapor pressures in Mackay et al. (2006) and considering the different vapor pressures at different temperatures (e.g. 20 °C vs. 25 °C), the values agree with each other within a factor of 5 for the two compounds.

Moreover, we found that most of the values listed in Mackay et al. (2006) are cited from previous estimates or compilations in various handbooks or databases. Schwarzenbach et al. (1988) provides the only direct measurement for 4-nitrophenol. In addition to Schwarzenbach et al. (1988), the other measurement result for 2,4-dinitrophenol was from Hoyer and Peperle (1958). This early measurement (Hoyer and Peperle, 1958) was published in German and we have no clue on the robustness of the reported solid vapor pressure due to the language barrier. Schwarzenbach et al. (1988) reported the direct measurements of the sub-cooled vapor pressures of 4-nitrophenol, 2,4-dinitrophenol and other nitrated phenols at different temperatures. Thus, Schwarzenbach et al. (1988) provides the most comprehensive results for the vapor pressures of nitrated phenols and is preferred to be used in this study. We agree with the reviewer that the measurements in Schwarzenbach et al. (1988) may need additional validation from other independent measurements. We added the information in the revised manuscript.

**Although vapor pressures from Schwarzenbach et al. (1988) might have significant uncertainties, Schwarzenbach et al. (1988) provided the only comprehensive measurements of sub-cooled liquid vapor pressures of nitrated phenols reported in the literature.**

2. P11 L25 Which hydrocarbons were measured and used for the simulation. It would be nice to show a table in the supplement with characteristic concentrations.

Reply: We added a table in the supplement (Table S2) to show the averages and standard deviations of measured concentrations of VOCs, NO<sub>x</sub> and ozone, which were used for constraints in the box model simulations in Jan. 18-Jan. 27 during UBWOS 2014 campaign.

**3. P12L10.** What was the assumption with respect to an emission rate of benzene?

Reply: Benzene was mainly emitted from oil and gas activities during the UBWOS campaigns. The variations of emission rates of benzene, CH<sub>4</sub> and other VOCs at different time of the day are expected to be small (Koss et al., 2015). Thus, the lower concentrations of benzene and CH<sub>4</sub> in the afternoon indicate a higher physical loss rate (i.e. dilution) at this time of day, in accordance with previous modeling studies for the UBWOS campaigns (Edwards et al., 2014; Yuan et al., 2015).

**4. P13 L25** Vinylfuran was detected in biomass burning (Stockwell et al., 2015), but very low BB influence was claimed in this study. What is the source of vinylfuran and why is it not present in the daytime?

Reply: Vinylfuran has the same molecular formula as phenol. We suspect vinylfuran might be an interference for phenol measurements and it may account for the difference between measured and modeled phenol concentrations. However, we have no information from the measurements for the source of this potential interference.

**5. (A)** Perhaps the online GC-MS used in this study can give some insight on the interference at mass 138.

Reply: The comment #5 is a long comment. We have divided the comment into six small comments (A-F) (see below) and we will deal with them one by one.

**(A)** We would like to clarify that there is no evidence for an interference to the NP measurement at mass 138 of the acetate ToF-CIMS during UBWOS 2014.

**(B)** The C<sub>3</sub>H<sub>4</sub>F<sub>2</sub>OH<sup>+</sup> ion that overlaps with the phenol peak (Fig. 2d) looks a little unusual. Does it come from the heated Teflon inlet? It would be useful to show the zero air signal with this ion to demonstrate this.

Reply: We checked the instrument background signals of C<sub>3</sub>H<sub>4</sub>F<sub>2</sub>OH<sup>+</sup> ion in PTR-TOF. The background signals decreased gradually during the measurements period. The

ambient signals of  $\text{C}_3\text{H}_4\text{F}_2\text{OH}^+$  were not significantly larger than the instrument background. Taken together, we believe  $\text{C}_3\text{H}_4\text{F}_2\text{OH}^+$  signals were the result of continuous fluxes from instrument walls. As no inlet switching was performed for PTR-TOF during UBWOS 2014, it is not possible to determine whether it is solely from sampling inlet.

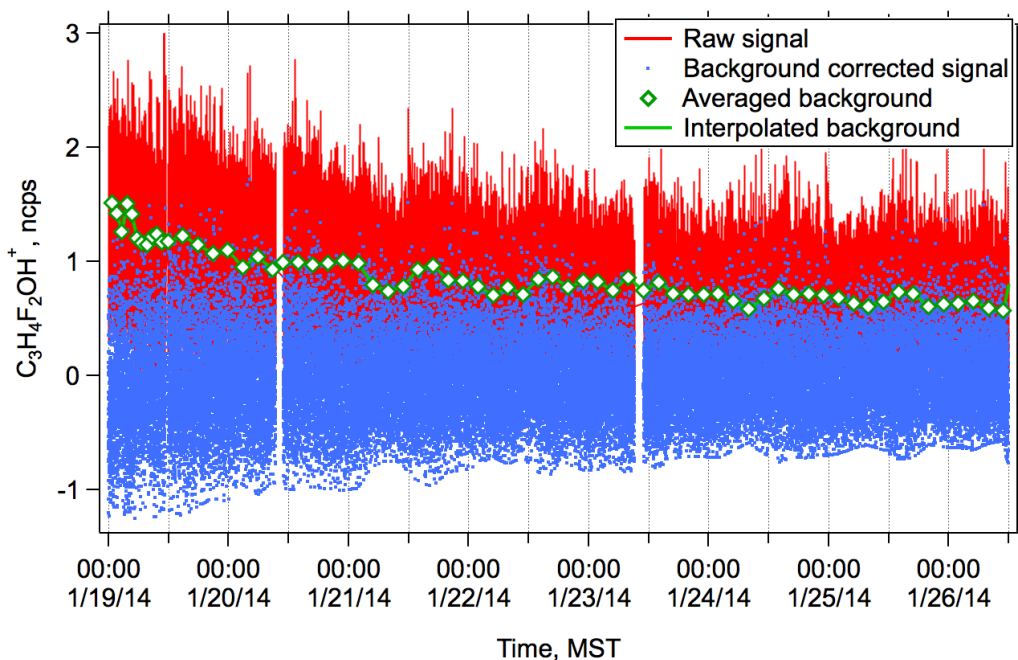


Figure R1. Time series of the raw signals, averaged background signals, interpolated background signals and background-corrected signals for the  $\text{C}_3\text{H}_4\text{F}_2\text{OH}^+$  ion in PTR-TOF during UBWOS 2014. The background-corrected signal is symmetrically scattered around zero, indicating no measurable signal in ambient air.

(C) Figure S2a, b, c show a large number of radical species measured. Since the acetate ionization technique is a soft method, some explanation is necessary about the source of these radicals. Is it because of the strong voltage used in the declustering region?

Reply: The ions observed in acetate CIMS are mainly from the proton abstraction of the targeted acids. Ions without deprotonation were also observed at low intensities in acetate TOF-CIMS. Examples for this are the ions with only C, H and O in the formula (e.g.  $\text{C}_8\text{H}_{10}\text{O}_2^-$  at  $m/z$  138) at even masses. These ions without deprotonation are believed to be from electron transfer reactions and/or fragmentation (Stark et al., 2015). We do not expect that atmospheric radicals contributed significantly to the signals of the ions without deprotonation.

**(D)** It would be useful to show the peaks at  $m/z$  137 along with the peaks at  $m/z$  138 in figure 2a in order to show that the peaks at 138 are not the C13 isotopes.

Reply: The isotopes from lower masses were always taken into account in the high-resolution peak fitting to the mass spectra in UBWOS 2014. The isotope signals from lower masses are shown as dark green curves in Figure 2 in the revised manuscript (also in Figure R2 below). These isotope signals were subtracted from the measured signals at each  $m/z$ , and then peak fitting to the mass was performed (Stark et al., 2015). Based on Figure 2 in the revised manuscript, isotope signals from lower masses only accounted for minor fractions of the measured signals at  $m/z$  138 and other  $m/z$  in revised Figure 2.

**(E)** According to P8 L26 the error in peak fitting was 0-10%, according to figure S2 the DNP peak area account for about 3% of the whole peak area at  $m/z$  183 (DNP peak height 10% from the total peak height and peak width about 1/3 of the total peak width), therefore the area of the DNP peak is below the accuracy of the peak fitting. Some additional explanation about the accuracy of the peak fitting is needed.

Reply: The mass spectrum of  $m/z$  183 shown in Figure 2 (C) of the revised manuscript (also Figure R2 C) are the average from January 25, 2015, when the interference of DNP from  $C_3F_6HO_2^-$  ions was significant. The averaged mass spectrum of  $m/z$  183 from Jan. 18, when the interference from  $C_3F_6HO_2^-$  ions was small, is shown in Figure R2 (D). The errors of ion signals from HR peak fitting are dependent on the ratios of ion signals relative to its neighboring peaks (Cubison and Jimenez, 2015). It is clear that the ratios of the DNP signal ( $C_6H_3N_2O_5^-$ ) to  $C_3F_6HO_2^-$  signal on Jan. 18 was much larger than those in Jan. 25. Thus, only DNP measurements in Jan. 18-22 were used for the analysis in this study.

The precision and accuracy of peak fitting are affected by the ratios between the targeted peaks and their neighboring peaks. Smaller ratios of the signals between the targeted peak and its neighboring peaks have been shown to deteriorate the precision of fitted signals for the targeted peak (Cubison and Jimenez, 2015; Müller et al., 2011; Corbin et al., 2015). Based on the reviewers' comments, a more detailed discussion on peak-fitting uncertainties is added to the revised manuscript (see revisions after the response to

comment 5F).

**(F)** Figure 7 shows that the measured DNP concentration sometimes has a negative value, is it an artifact from the peak fitting procedure or background subtraction? Does the DNP peak area correlate with the area of the C<sub>8</sub>H<sub>7</sub>O<sub>5</sub><sup>-</sup> peak?

Reply: Negative values of DNP concentration in Figure 8 in the revised manuscript (Figure 7 in ACPD version) are due to background subtraction. The peak fitting by definition only returns positive values for different product ion signals. Averaging over a longer time would reduce the variations of concentrations at low levels.

Based on the collective reviewers' comments, we have expanded the discussion of peak-fitting in Section 2, including mass calibration and its error, interpretation of the mass spectra, discussions on the uncertainty of the fitted signals. The inlet issue for DNP presented in Section 3.3 is also moved to this part. A graph showing the sensitivity of fitted ion intensities to mass calibration errors is also included in the supplement (Figure S2). The added or modified paragraphs are:

**Post-measurement mass calibrations were performed using nine isolated ions, including m/z 31.9904 (O<sub>2</sub><sup>-</sup>), m/z 34.9694 (Cl<sup>-</sup>), m/z 44.9982 (CHO<sub>2</sub><sup>-</sup>), m/z 59.0139 (C<sub>2</sub>H<sub>3</sub>O<sub>2</sub><sup>-</sup>), m/z 61.9884 (NO<sub>3</sub><sup>-</sup>), m/z 143.9840 (C<sub>3</sub>F<sub>4</sub>O<sub>2</sub><sup>-</sup>), m/z 162.9824 (C<sub>3</sub>F<sub>5</sub>O<sub>2</sub><sup>-</sup>), m/z 193.9808 (C<sub>4</sub>F<sub>6</sub>O<sub>2</sub><sup>-</sup>) and m/z 243.9776 (C<sub>5</sub>F<sub>8</sub>O<sub>2</sub><sup>-</sup>). The four fluorine-containing ions in the list were released from Teflon inlet during UBWOS 2014 and their persistent presence was used for mass calibration. The accuracy of mass calibration was 4.7±1.9 ppm for the whole campaign and the errors of mass calibration for individual ions were usually within 10 ppm (average+3σ).**

**High-resolution (HR) peak fitting to m/z 138, m/z 152 and m/z 183 in the averaged mass spectra of ToF-CIMS on a typical day (January 25, 2014) are shown as examples in Figure 2. Isotope signals from lower masses (dark green lines) accounted for small fractions of the m/z signals. Multiple overlapping ion peaks were identified in the m/z channels. In addition to nitrated phenols, several ions without deprotonation were also present in the even m/z (e.g. C<sub>8</sub>H<sub>10</sub>O<sub>2</sub><sup>-</sup> at m/z 138), possibly due to electron transfer reactions and/or fragmentation in the quadrupole**

ion guides (Stark et al., 2015). The signals of NP and MNP were either the largest or significant larger than their neighboring peaks at their respective  $m/z$ , whereas the signal of DNP was much smaller than its neighboring peaks on January 25, 2014. Smaller ratios of the signals between the targeted peak and its neighboring peaks have been shown to deteriorate the precision of fitted signals for the targeted peak (Cubison and Jimenez, 2015; Müller et al., 2011; Corbin et al., 2015). Based on the provided equations in Cubison and Jimenez (2015), the imprecision arising from mass calibration (not including counting error) for the signals of NP, MNP and DNP are 3.2%, 1.8% and 47% based on the mass spectra of January 25, respectively. Imperfect mass calibration can also affect fitted magnitudes of ion signals. Figure S2 shows the sensitivity of the fitted signals of various masses as a function of the errors in mass calibration. The signal changes at a 10 ppm (average+ $3\sigma$ ) error of mass calibration relative to perfect mass calibration (error=0 ppm) for NP, MNP and DNP signals are as high as 14%, 5% and 81%, respectively. The results from both precision calculation and sensitivity of fitted magnitudes indicate that the peak signals of NP and MNP can be fitted well with low uncertainties. The peak fitting at  $m/z$  166 for DMNP shows similar results as  $m/z$  138 for NP and  $m/z$  152 for MNP. However, large uncertainties are associated with the peak signals of DNP on January 25, 2014, which is mainly affected by the  $C_3F_6HO_2^-$  ions ( $m/z$  182.9886) as indicated by the opposite behaviors of the DNP ion and  $C_3F_6HO_2^-$  ion in Figure S2C.

The  $C_3F_6HO_2^-$  ion ( $m/z$  182.9886) was released from the heated Teflon inlet along with other fluorine-containing ions that were used for mass calibration. The release of  $C_3F_6HO_2^-$  ion was supported by much higher signals from the long-heated inlet compared to the short-unheated inlet, when inlet-switching experiments were conducted in February 2-5 (Figure S1). Long-heated inlets were used for most of the time during UBWOS 2014 (January 23- February 13), except during January 18-22, when a short-unheated inlet was used. The averaged mass spectra of  $m/z$  183 measured on January 18 is shown in Figure 2D. Compared to the mass spectra on January 25,  $C_3F_6HO_2^-$  signals on January 18 were lower and the signals of DNP were larger than of  $C_3F_6HO_2^-$  ions. As a result, the uncertainty from peak fitting for the DNP ion was much lower on January 18 (Figure S2D). Thus, we will only use

measured DNP data in the beginning of the campaign (January 18-22), when the long heated inlet was not connected to the acetate CIMS and no inlet switching was performed.

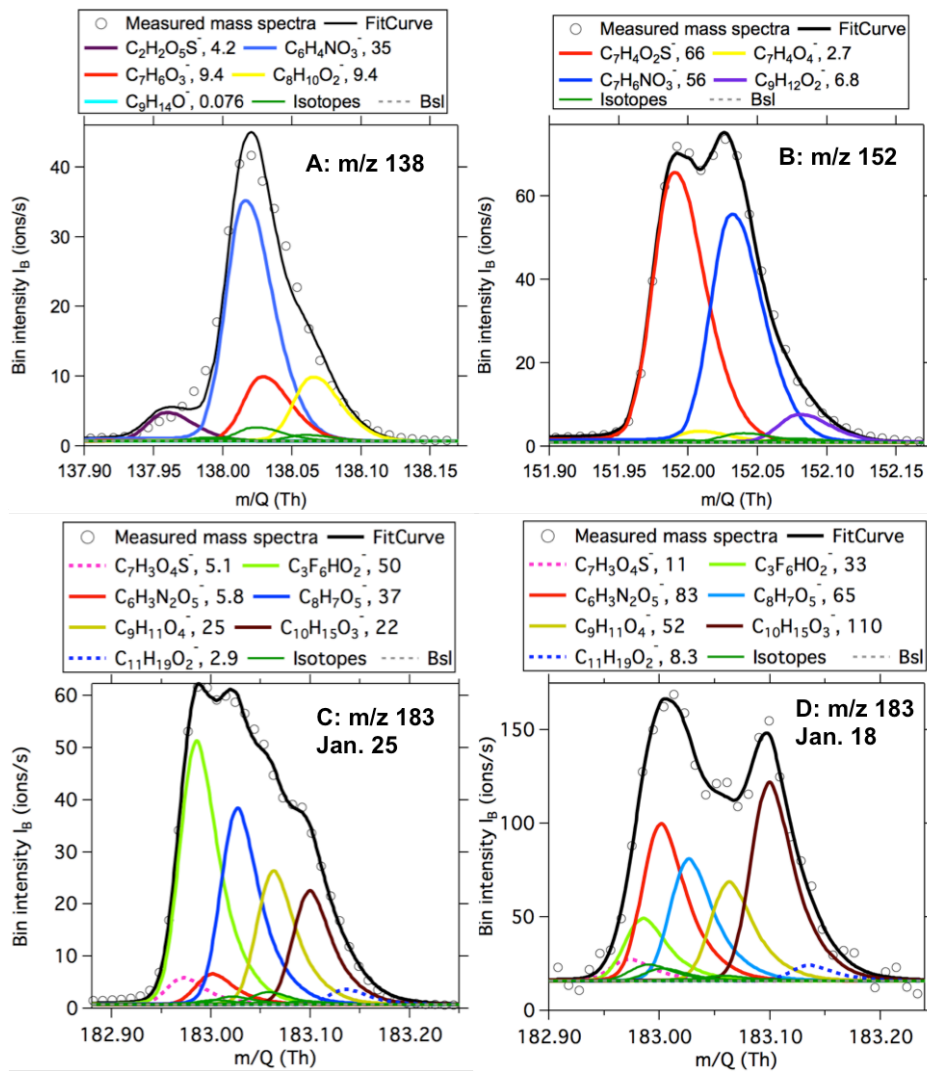


Figure R2 (Figure 2 in the revised manuscript). High-resolution peak fitting to the averaged mass spectra of acetate ToF-CIMS for  $m/z$  138 (A),  $m/z$  152 (B) and  $m/z$  183 (C) on January 25, 2014 and  $m/z$  183 (D) on Jan. 18, 2014 during UBWOS 2014. The dark green lines indicate the calculated isotope signals from lower masses.



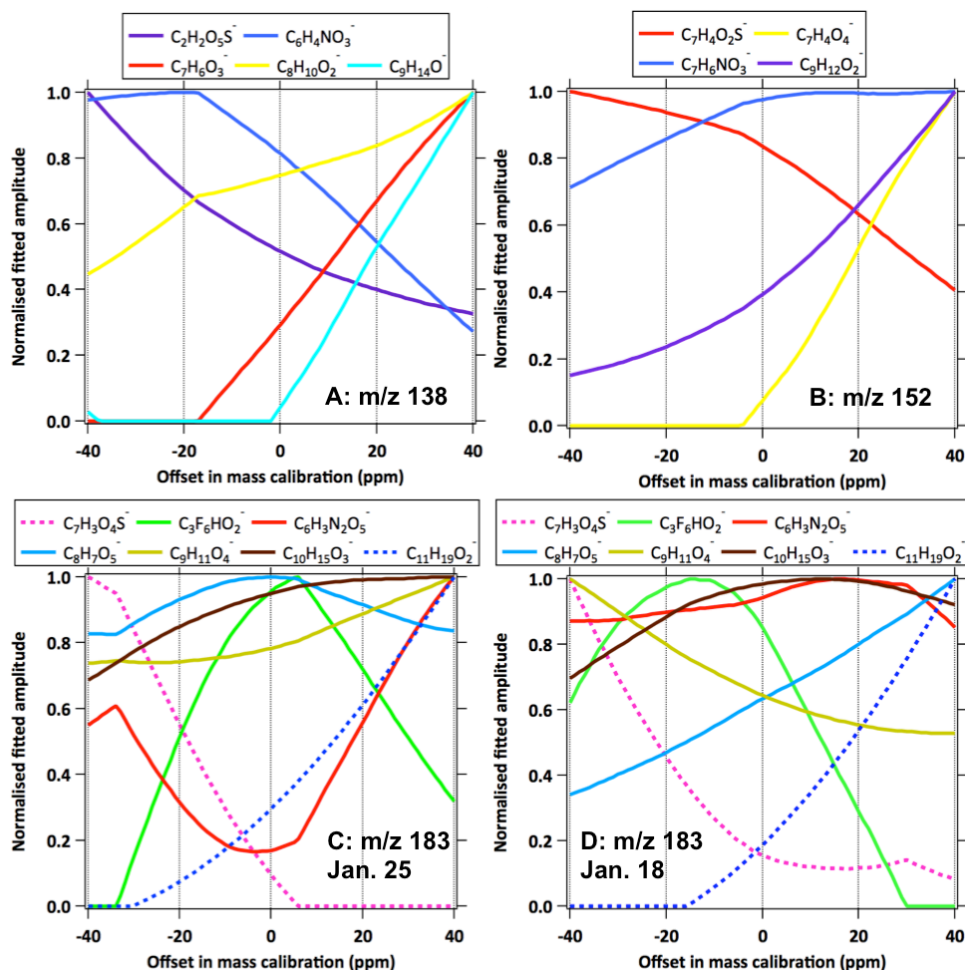


Figure R3 (Figure S2 in the revised manuscript). Sensitivity of the fitted ion intensities to mass calibration errors for ions at  $m/z$  138 (A),  $m/z$  152 (B) and  $m/z$  183 (C) based on the averaged mass spectra on January 25, 2014 and  $m/z$  183 (D) based on the averaged mass spectra on January 18, 2014 (see mass spectra in Figure 2). The results in the plots were obtained by (1) shifting the measured mass spectra by varying amount (from -40 ppm to 40 ppm) and (2) conducting peak fitting to the shifted mass spectra using the same ion locations calculated from their formula (Stark et al., 2015). The fitted signals relative to the maximum signals obtained between -40 ppm and 40 ppm are shown for each individual ion. The accuracy of mass calibration was  $4.7 \pm 1.9$  ppm for the whole campaign and the errors of mass calibration for individual ions were usually within 10 ppm (average+ $3\sigma$ ).

P7 L6 What was the length of the short inlet?

Reply: The length of the short inlet used during February 1-5 was around 2 meters. We added this information in the revised manuscript.

Technical: P36 fig 5 What is the line for the G/P partitioning using 4-NP?

Reply: The legend of Figure 5 in ACPD version is updated in the revised manuscript to better convey the information. The green solid line is the modeled gas-phase concentration from the G/P partitioning using 4-NP. The updated graph is shown below.

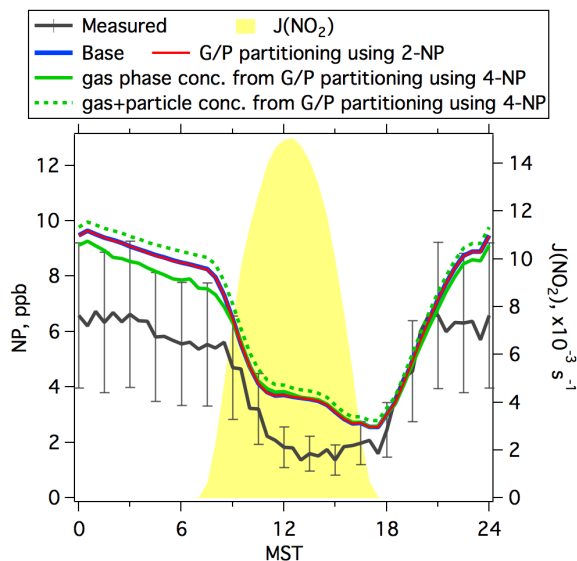


Figure R4. Diurnal profiles of measured and modeled concentrations of NP from the base simulation and the simulations considering gas/particle partitioning. Photolysis frequencies of NO<sub>2</sub> are shown for reference. Error bars indicate the accuracies of concentrations of NP (40%).

## **Anonymous Referee #2**

This manuscript describes some novel measurements of nitrated phenols made in the Uintah Basin late January into early February, 2014. The measurements themselves are novel and indicate a high sensitivity and reasonable specificity for the target species. The measurements are complemented by a fairly simple modeling exercise, which shows that the data can be fitted by a chemical model accompanied by deposition and dilution terms without too much tweaking. Overall, this is a valuable study, which can be published without too many changes. The measurements are fairly novel, and perhaps would benefit from a little more discussion.

[Reply: We would like to thank the reviewer for these valuable comments.](#)

The figures showing mass spectral peak-fitting are central to understanding the quality of the data, but are relegated to Supplemental Material. I would like to see them featured more prominently, and with some further discussion. For example, how variable are the other signals shown in Figures S2 (A-D)? What are the proposed identities of some of the other peaks, and do they show similar diurnal profiles? For that matter, when were the shown spectra taken (date, time of day)? A little more information along these lines would help others to assess the reliability and generality of the technique.

On the other hand, quite a lot of space is devoted to the model, which does not really bring a whole lot of insight to the chemistry. Admittedly, it is shown that the modeled diurnal profiles match the measurements quite well, but it is after all “only” a box model, and transport and dilution are treated simplistically. However, the interpretation of the model does not overstep its limits, and the exercise is useful, if only in showing that the measured diurnal profiles are reasonable.

[Reply: We agree with the reviewer that high-resolution peak fitting to the mass spectra is essential for the quality of the results presented in this study. The uncertainties due to high-resolution peak fitting have been discussed in several recent papers \(Corbin et al., 2015; Cubison and Jimenez, 2015; Müller et al., 2011\). We moved the mass spectra plots from the supplemental information to the main text in the revised manuscript. The mass spectra in the plots \(Figure 2 in the revised manuscript\) were averaged from the mass spectra measured on January 25 \(and also January 18 in the Figure 2D\). As shown in](#)

Figure 5 in the revised manuscript, January 25 was a typical measurement day during the UBWOS campaign, with similar concentrations of nitrated phenols as the campaign averages shown in Figure 3. Thus, they are representative for the peak-fitting issues encountered during UBWOS 2014. Based on the reviewer's comments and also comments from reviewer #1, we have expanded the discussions of peak fitting in Section 2, including mass calibration and its error, interpretation of the mass spectra, discussions on the uncertainty of the fitted signals. The inlet issue for DNP presented in Section 3.3 is also moved to this part. A graph showing the sensitivity of fitted ion intensities to mass calibration errors is also included in the supplement (Figure S2). The added and modified paragraphs are (same revision as described in our response to Reviewer 1):

**Post-measurement mass calibrations were performed using nine isolated ions, including  $m/z$  31.9904 ( $O_2^-$ ),  $m/z$  34.9694 ( $Cl^-$ ),  $m/z$  44.9982 ( $CHO_2^-$ ),  $m/z$  59.0139 ( $C_2H_3O_2^-$ ),  $m/z$  61.9884 ( $NO_3^-$ ),  $m/z$  143.9840 ( $C_3F_4O_2^-$ ),  $m/z$  162.9824 ( $C_3F_5O_2^-$ ),  $m/z$  193.9808 ( $C_4F_6O_2^-$ ) and  $m/z$  243.9776 ( $C_5F_8O_2^-$ ). The four fluorine-containing ions in the list were released from Teflon inlet during UBWOS 2014 and their persistent presence was used for mass calibration. The accuracy of mass calibration was  $4.7 \pm 1.9$  ppm for the whole campaign and the errors of mass calibration for individual ions were usually within 10 ppm (average+ $3\sigma$ ).**

High-resolution (HR) peak fitting to  $m/z$  138,  $m/z$  152 and  $m/z$  183 in the averaged mass spectra of ToF-CIMS on a typical day (January 25, 2014) are shown as examples in Figure 2. Isotope signals from lower masses (dark green lines) accounted for small fractions of the  $m/z$  signals. Multiple overlapping ion peaks were identified in the  $m/z$  channels. In addition to nitrated phenols, several ions without deprotonation were also present in the even  $m/z$  (e.g.  $C_8H_{10}O_2^-$  at  $m/z$  138), possibly due to electron transfer reactions and/or fragmentation in the quadrupole ion guides (Stark et al., 2015). The signals of NP and MNP were either the largest or significant larger than their neighboring peaks at their respective  $m/z$ , whereas the signal of DNP was much smaller than its neighboring peaks on January 25, 2014. Smaller ratios of the signals between the targeted peak and its neighboring peaks have been shown to deteriorate the precision of fitted signals for the targeted peak (Cubison and Jimenez, 2015; Müller et al., 2011; Corbin et al., 2015). Based on the

provided equations in Cubison and Jimenez (2015), the imprecision arising from mass calibration (not including counting error) for the signals of NP, MNP and DNP are 3.2%, 1.8% and 47% based on the mass spectra of January 25, respectively. Imperfect mass calibration can also affect fitted magnitudes of ion signals. Figure S2 shows the sensitivity of the fitted signals of various masses as a function of the errors in mass calibration. The signal changes at a 10 ppm (average+3 $\sigma$ ) error of mass calibration relative to perfect mass calibration (error=0 ppm) for NP, MNP and DNP signals are as high as 14%, 5% and 81%, respectively. The results from both precision calculation and sensitivity of fitted magnitudes indicate that the peak signals of NP and MNP can be fitted well with low uncertainties. The peak fitting at m/z 166 for DMNP shows similar results as m/z 138 for NP and m/z 152 for MNP. However, large uncertainties are associated with the peak signals of DNP on January 25, 2014, which is mainly affected by the  $C_3F_6HO_2^-$  ions (m/z 182.9886) as indicated by the opposite behaviors of the DNP ion and  $C_3F_6HO_2^-$  ion in Figure S2C.

The  $C_3F_6HO_2^-$  ion (m/z 182.9886) was released from the heated Teflon inlet along with other fluorine-containing ions that were used for mass calibration. The release of  $C_3F_6HO_2^-$  ion was supported by much higher signals from the long-heated inlet compared to the short-unheated inlet, when inlet-switching experiments were conducted in February 2-5 (Figure S1). Long-heated inlets were used for most of the time during UBWOS 2014 (January 23- February 13), except during January 18-22, when a short-unheated inlet was used. The averaged mass spectra of m/z 183 measured on January 18 is shown in Figure 2D. Compared to the mass spectra on January 25,  $C_3F_6HO_2^-$  signals on January 18 were lower and the signals of DNP were larger than of  $C_3F_6HO_2^-$  ions. As a result, the uncertainty from peak fitting for the DNP ion was much lower on January 18 (Figure S2D). Thus, we will only use measured DNP data in the beginning of the campaign (January 18-22), when the long heated inlet was not connected to the acetate CIMS and no inlet switching was performed.

1. Specific comments: There are a few spots in the manuscript where the grammar needs tightening up. E.g., P28662, line 16. “oxidation... with nitration process...” P28666, lines 7-20. Repeats discussion of acetic anhydride. Also, it wasn’t totally clear whether you

were talking about your own IMR, or comparing to others. P28670, line 10. “inertial” should be “inert” ?

Reply: P28662 line 16: the sentence is changed to: **Further oxidation of nitrated phenols by obtaining another nitro- group produces dinitrophenols (DNP).**

P28666 line 7-20: “The different sensitivity ratios of 4-NP/2-NP between our instrument and that in Mohr et al. (2013) can be caused by many different instrumental conditions” is changed to “**The different sensitivity ratios of 4-NP/2-NP can be caused by many different instrumental conditions between our instrument and that in Mohr et al. (2013)**”.

P28670 line 10: Changed.

2. P28670, model tests in Fig S3. Was the photolysis to give phenoxy + NO<sub>2</sub> the only channel included? Since this channel reforms NP, you can't really rule out its occurrence concurrently with HONO production, since as you say it would be a null channel. Since the overall quantum yield is only about 1E-3, there is a lot of room for parallel channels occurring. Admittedly, though, Bejan et al. (2006) point out that photolysis of 2.5 ppm 3-methyl-2-nitrophenol led to <0.14 ppb NO<sub>2</sub>, so the channel is probably only small.

Reply: We are thankful for the reviewer's comments. The model tests presented in Figure S3 in the ACPD version (Figure S4 in the revised manuscript) assumes the photolysis only gives phenoxy + NO<sub>2</sub>. From our simulation test, we concluded this photolysis pathway is not an effective loss for NP.

We agree with the reviewer that this pathway may still occur concurrently with the pathway forming HONO + 2-phenoxy biradicals. As the photolysis rate of NP in Bardini (2006) was derived from the change of NP concentrations in a chamber associated with OH scavenger, the photolysis rate determined in Bardini (2006) may not include this pathway even though it may be happening. We added this discussion in the revised manuscript.

**The simulation test in Figure S3 indicates that the pathway forming C<sub>6</sub>H<sub>5</sub>O radicals and NO<sub>2</sub> is an ineffective sink for NP, since C<sub>6</sub>H<sub>5</sub>O radical will re-form NP by reacting with NO<sub>2</sub>. However, we cannot exclude this pathway to occur along with**

**that producing 2-phenoxy biradicals and HONO. The photolysis frequency determined in Bardini (2006) from concentration changes of 2-nitrophenol in a chamber may not include this pathway as well. As a result, attributing the photolysis rates determined in Bardini (2006) to other pathways other than Route2 is reasonable.**

3. P28671, lines 17-22. What is the rationale for assuming that the interference is only present during the night? How would alternative assumptions affect the conclusions from the model?

Reply: The modeled phenol concentrations agreed reasonably well with measurements during the daytime, but significant disagreement was observed at night. One possible explanation is a chemical interference of phenol that is only present. We cannot rule out that such an interference was also present in the daytime. If similar magnitudes of interferences also occurred in the daytime, modeled phenol concentrations would be higher than measurements in the daytime, but still in the combined uncertainty of measurement and the model in this period.

4. P28675. Presumably the reaction of OH with phenol is such a small contributor to NP production because the OH mostly adds to the ring? Maybe a comment would help to clarify this. It is interesting that so many sources of C<sub>6</sub>H<sub>5</sub>O<sub>2</sub> (and consequently, C<sub>6</sub>H<sub>5</sub>O) exist. Of the flux through C<sub>6</sub>H<sub>5</sub>O<sub>2</sub> + NO, only about a third makes NP. Is this because phenoxy radicals cycle back to RO<sub>2</sub> through the O<sub>3</sub> reaction? How does the inclusion of the phenoxy + NO reaction affect the phenoxy and NP budgets around midday? Interpretation of these figures might be a little easier if the NO<sub>2</sub> and O<sub>3</sub> levels were given somewhere.

Reply: The reaction of OH with phenol mainly happens through OH addition, ultimately forming catechol (yield=80% in MCM). The yield of NP from the reaction of OH with phenol is only 6% in MCM. We added this information in the revised manuscript.

**The reaction of phenol with OH radicals only accounts for a small fraction of the production of C<sub>6</sub>H<sub>5</sub>O radicals (2% for 24-hour average), due to the small yield of NP (6%) from the reaction of OH with phenol in the MCM.**

Most of the phenoxy radicals formed from the  $C_6H_5O_2+NO$  reaction recycle back to  $C_6H_5O_2$  radicals through its reaction with  $O_3$ . Based on Figure 7 (B and C) in the revised manuscript, only about of a third of  $C_6H_5O$  radicals form NP. The production of  $C_6H_5O$  radicals is not affected by the inclusion of the  $C_6H_5O+NO$  reaction. The inclusion of the  $C_6H_5O+NO$  reaction reduces formation rates of NP in the noontime, as the loss of  $C_6H_5O$  is higher and the steady-state concentration of  $C_6H_5O$  is lower in the midday. The average concentrations of NO,  $NO_2$  and  $O_3$  in Jan. 18-Jan.27 during UBWOS 2014 are shown in a table (Table S2) in the supplement in the revised manuscript. The discussions on the effects of  $C_6H_5O + NO$  reaction to NP budget are added in the revised manuscript.

**The inclusion of the reaction of phenoxy radicals ( $C_6H_5O$ ) with NO discussed in section 3.2.2 would mainly affect NP budget in the noontime, with smaller production and loss in this period.**

5. P28676, line 17. Just to clarify; you mean 100% of nitrated phenols that are actually lost by photolysis (since the overall quantum yield is  $<1E-3$ ).

Reply: Here, we mean that each molecule of nitrated phenols lost by photolysis (the rate is  $1.4\% \times J(NO_2)$ ) yields one HONO molecule. We changed the sentence slightly in the revised manuscript to make it clearer.

**“If we assume photolysis of nitrated phenols at rates of  $1.4\% \times J(NO_2)$  yields HONO at a 100% yield (upper limit),...”**

6. Figure 5, caption. Delete “in (b) and (d)”.

Reply: Done.



## References:

- Bardini, P.: Atmospheric Chemistry of Dimethylphenols & Nitrophenols, PhD, University College Cork, Corcaigh, 2006.
- Cappa, C. D., Lovejoy, E. R., and Ravishankara, A. R.: Evidence for liquid-like and nonideal behavior of a mixture of organic aerosol components, *Proc Natl Acad Sci U S A*, 105, 18687-18691, 10.1073/pnas.0802144105, 2008.
- Corbin, J., Othman, A., D. Allan, J., R. Worsnop, D., D. Haskins, J., Sierau, B., Lohmann, U., and A. Mensah, A.: Peak-fitting and integration imprecision in the Aerodyne aerosol mass spectrometer: effects of mass accuracy on location-constrained fits, *Atmospheric Measurement Techniques*, 8, 4615-4636, 10.5194/amt-8-4615-2015, 2015.
- Cubison, M. J., and Jimenez, J. L.: Statistical precision of the intensities retrieved from constrained fitting of overlapping peaks in high-resolution mass spectra, *Atmospheric Measurement Techniques*, 8, 2333-2345, 10.5194/amt-8-2333-2015, 2015.
- Edwards, P. M., Brown, S. S., Roberts, J. M., Ahmadov, R., Banta, R. M., deGouw, J. A., Dube, W. P., Field, R. A., Flynn, J. H., Gilman, J. B., Graus, M., Helmig, D., Koss, A., Langford, A. O., Lefer, B. L., Lerner, B. M., Li, R., Li, S. M., McKeen, S. A., Murphy, S. M., Parrish, D. D., Senff, C. J., Soltis, J., Stutz, J., Sweeney, C., Thompson, C. R., Trainer, M. K., Tsai, C., Veres, P. R., Washenfelder, R. A., Warneke, C., Wild, R. J., Young, C. J., Yuan, B., and Zamora, R.: High winter ozone pollution from carbonyl photolysis in an oil and gas basin, *Nature*, 514, 351-354, 10.1038/nature13767, 2014.
- Hoyer, v. H., and Peperle, W.: Dampfdruckmessungen an organischen Substanzen und ihre Sublimationswärmen, *Zeitschrift für Elektrochemie, Berichte der Bunsengesellschaft für physikalische Chemie*, 62, 61-66, 1958.
- Koss, A. R., de Gouw, J., Warneke, C., Gilman, J. B., Lerner, B. M., Graus, M., Yuan, B., Edwards, P., Brown, S. S., Wild, R., Roberts, J. M., Bates, T. S., and Quinn, P. K.: Photochemical aging of volatile organic compounds associated with oil and natural gas extraction in the Uintah Basin, UT, during a wintertime ozone formation event, *Atmospheric Chemistry and Physics*, 15, 5727-5741, 10.5194/acp-15-5727-2015, 2015.
- Mackay, D., Shiu, W.-Y., Ma, K.-C., and Lee, S. C.: *Handbook of physical-chemical properties and environmental fate for organic chemicals*, CRC press, 2006.
- Müller, M., George, C., and D'Anna, B.: Enhanced spectral analysis of C-TOF Aerosol Mass Spectrometer data: Iterative residual analysis and cumulative peak fitting, *International Journal of Mass Spectrometry*, 306, 1-8, <http://dx.doi.org/10.1016/j.ijms.2011.04.007>, 2011.
- Schwarzenbach, R. P., Stierli, R., Folsom, B. R., and Zeyer, J.: Compound properties relevant for assessing the environmental partitioning of nitrophenols, *Environmental Science & Technology*, 22, 83-92, 10.1021/es00166a009, 1988.
- Stark, H., Yatavelli, R. L. N., Thompson, S. L., Kimmel, J. R., Cubison, M. J., Chhabra, P. S., Canagaratna, M. R., Jayne, J. T., Worsnop, D. R., and Jimenez, J. L.: Methods

- to extract molecular and bulk chemical information from series of complex mass spectra with limited mass resolution, *International Journal of Mass Spectrometry*, 10.1016/j.ijms.2015.08.011, 2015.
- Yatavelli, R. L. N., Stark, H., Thompson, S. L., Kimmel, J. R., Cubison, M. J., Day, D. A., Campuzano-Jost, P., Palm, B. B., Hodzic, A., Thornton, J. A., Jayne, J. T., Worsnop, D. R., and Jimenez, J. L.: Semicontinuous measurements of gas-particle partitioning of organic acids in a ponderosa pine forest using a MOVI-HRToF-CIMS, *Atmos. Chem. Phys.*, 14, 1527-1546, 10.5194/acp-14-1527-2014, 2014.
- Yuan, B., Veres, P. R., Warneke, C., Roberts, J. M., Gilman, J. B., Koss, A., Edwards, P. M., Graus, M., Kuster, W. C., Li, S. M., Wild, R. J., Brown, S. S., Dubé, W. P., Lerner, B. M., Williams, E. J., Johnson, J. E., Quinn, P. K., Bates, T. S., Lefer, B., Hayes, P. L., Jimenez, J. L., Weber, R. J., Zamora, R., Ervens, B., Millet, D. B., Rappenglück, B., and de Gouw, J. A.: Investigation of secondary formation of formic acid: urban environment vs. oil and gas producing region, *Atmos. Chem. Phys.*, 15, 1975-1993, 10.5194/acp-15-1975-2015, 2015.

1     **Secondary formation of nitrated phenols: insights from observations**  
2             **during the Uintah Basin Winter Ozone Study (UBWOS) 2014**

3     Bin Yuan<sup>1,2</sup>, John Liggio<sup>3</sup>, Jeremy Wentzell<sup>3</sup>, Shao-Meng Li<sup>3</sup>, Harald Stark<sup>2,4</sup>, James M.  
4     Roberts<sup>1</sup>, Jessica Gilman<sup>1,2</sup>, Brian Lerner<sup>1,2</sup>, Carsten Warneke<sup>1,2</sup>, Rui Li<sup>1,2</sup>, Amy  
5     Leithead<sup>3</sup>, Hans D. Osthoff<sup>5</sup>, Robert Wild<sup>1,2</sup>, Steven S. Brown<sup>1,6</sup>, and Joost A. de  
6     Gouw<sup>1,2,6</sup>

7     1. NOAA Earth System Research Laboratory (ESRL), Chemical Sciences Division,  
8     Boulder, CO, USA

9     2. Cooperative Institute for Research in Environmental Sciences, University of Colorado  
10    at Boulder, Boulder, CO, USA

11    3. Environment Canada, Science and Technology Branch, Toronto, ON, Canada

12    4. Aerodyne Research Inc., Billerica, MA, USA

13    5. Department of Chemistry, University of Calgary, Calgary, Canada

14    6. Department of Chemistry and Biochemistry, University of Colorado at Boulder, CO,  
15    USA

16

17

18 **Abstract**

19 We describe the results from online measurements of nitrated phenols using a time  
20 of flight chemical ionization mass spectrometer (ToF-CIMS) with acetate as reagent ion  
21 in an oil and gas production region in January and February of 2014. Strong diurnal  
22 profiles were observed for nitrated phenols, with concentration maxima at night. Based  
23 on known markers ( $\text{CH}_4$ ,  $\text{NO}_x$ ,  $\text{CO}_2$ ), primary emissions of nitrated phenols were not  
24 important in this study. A box model was used to simulate secondary formation of  
25 phenol, nitrophenol (NP) and dinitrophenols (DNP). The box model results indicate that  
26 oxidation of aromatics in the gas phase can explain the observed concentrations of NP  
27 and DNP in this study. Photolysis was the most efficient loss pathway for NP in the gas  
28 phase. We show that aqueous-phase reactions and heterogeneous reactions were minor  
29 sources of nitrated phenols in our study. This study demonstrates that the emergence of  
30 new ToF-CIMS (including PTR-TOF) techniques allows for the measurement of  
31 intermediate oxygenates at low levels and these measurements improve our  
32 understanding of the evolution of primary VOCs in the atmosphere.

33

## 34 1. Introduction

35 Nitrated phenols are a family of aromatic compounds with both nitro (-NO<sub>2</sub>) and  
36 hydroxyl groups (-OH) connected to a benzene ring. Nitrated phenols have been detected  
37 in the gas phase, aerosol, cloud water and rainwater (Harrison et al., 2005a). Many  
38 studies have shown that nitrated phenols are one of the important components of brown  
39 carbon in aerosol (Desyaterik et al., 2013; Mohr et al., 2013; Zhang et al., 2013; Lin et al.,  
40 2015), as they absorb light in the atmosphere (Bejan et al., 2007). Photolysis of some  
41 nitrated phenols was reported to produce nitrous acid (HONO) (Bejan et al., 2006) and  
42 hydroxyl (OH) radicals (Cheng et al., 2009), while the oxidation and photolysis of them  
43 contribute to secondary organic aerosol (SOA) formation, especially in biomass burning  
44 plumes (Mohr et al., 2013; Kitanovski et al., 2012; Lauraguais et al., 2014). There is also  
45 evidence that nitrated phenols are phytotoxic and contribute to forest decline (Rippen et  
46 al., 1987; Natangelo et al., 1999). Some nitrated phenols are known to be mutagenic and  
47 are of concern to human health (Fernandez et al., 1992).

48 Sources of nitrated phenols in the atmosphere include emissions from vehicle  
49 exhaust (Inomata et al., 2013; Tremp et al., 1993; Sekimoto et al., 2013) and biomass  
50 burning (Mohr et al., 2013). Nitrated phenols are also produced from photooxidation of  
51 aromatic hydrocarbons in the atmosphere: for example benzene oxidizes to 2-nitrophenol  
52 (2-NP) and 4-nitrophenol (4-NP), and toluene oxidizes to methylnitrophenols (MNP)  
53 (Harrison et al., 2005a). Figure 1 shows the reactions leading to secondary formation of  
54 NP and dinitrophenols (DNP) in the atmosphere (Jenkin et al., 2003). Oxidation of  
55 benzene by OH radicals forms phenol and further reactions of phenol with either OH or  
56 NO<sub>3</sub> radicals yield phenoxy (C<sub>6</sub>H<sub>5</sub>O) radicals, which react further with NO<sub>2</sub> to generate  
57 NP. In addition to benzene oxidation, C<sub>6</sub>H<sub>5</sub>O radical is also generated from the reaction  
58 of NO with phenyl peroxy (C<sub>6</sub>H<sub>5</sub>O<sub>2</sub>) radicals, a product from reactions of some other  
59 aromatic precursors, e.g. benzaldehyde (Caralp et al., 1999). Further oxidation of nitrated  
60 phenols by obtaining another nitro- group produces dinitrophenols (DNP). The yields of  
61 NP from phenol oxidation by OH radicals (Atkinson et al., 1992; Olariu et al.,  
62 2002; Berndt and Boge, 2003) and NO<sub>3</sub> radicals (Atkinson et al., 1992; Bolzacchini et al.,  
63 2001) have been reported. Berndt and Boge (2003) also showed that the NP yield from

Bin Yuan 12/25/2015 5:04 PM

**Deleted:** with nitration process

Bin Yuan 12/30/2015 1:15 PM

**Deleted:** will

66 OH oxidation of phenol increases at higher NO<sub>2</sub> concentrations. In addition to gas phase  
67 reactions, nitrated phenols are formed from aqueous-phase reactions in aerosol or cloud  
68 water (Vione et al., 2001, 2005). The importance of the aqueous reactions compared to  
69 gas-phase reactions is highly dependent on liquid water content in the atmosphere  
70 (Harrison et al., 2005b).

71 The sinks of nitrated phenols in the gas phase include reactions with OH radicals  
72 (Atkinson et al., 1992; Bejan et al., 2007), with NO<sub>3</sub> radicals (Atkinson et al., 1992), with  
73 chlorine atoms (Bejan et al., 2015) and photolysis (Bejan et al., 2007; Chen et al., 2011).  
74 It has been proposed that photolysis is the dominant gas phase atmospheric loss for  
75 nitrated phenols (Bejan et al., 2007). Despite the importance of photolysis of nitrated  
76 phenols, the photolysis frequency of nitrated phenols under ambient conditions was only  
77 reported in a single non-peer reviewed publication (1.4% of photolysis frequency of NO<sub>2</sub>)  
78 (Bardini, 2006). The chemical products from photolysis of nitrated phenols were  
79 proposed, but the proposed products were not fully evaluated against experimental results  
80 (Bejan et al., 2006). Nitrated phenols are also removed by various processes in the  
81 aqueous phase, including reactions with OH, NO<sub>3</sub> and photolysis (Vione et al., 2009).

82 Measurements of nitrated phenols have been mainly conducted using offline  
83 methods (Harrison et al., 2005a). Air samples are usually collected on filters or cartridges  
84 and then analyzed by liquid chromatography (LC) methods (Rubio et al., 2012; Harrison  
85 et al., 2005a; Delhomme et al., 2010). These detection methods are time-consuming and  
86 measurements as a function of the time of day are not usually possible (Delhomme et al.,  
87 2010). The lack of fast-response online measurements has prevented, at least partially, a  
88 thorough investigation of sources and sinks of nitrated phenols. Recently, Mohr et al.  
89 (2013) deployed a chemical ionization mass spectrometer (CIMS) using acetate as the  
90 reagent ion to measure nitrated phenols online in the particle phase in winter in London  
91 and based on their measurements the authors concluded that nitrated phenols were mainly  
92 from wood burning in this region of the atmosphere.

93 In this study, we conducted high time resolution measurements of nitrated phenols  
94 in the gas phase at a site in an oil and gas production region in winter. High  
95 concentrations of ozone and secondary products (Edwards et al., 2014) were observed at

96 this site, as the result of photochemical degradation of large amounts of alkanes and  
97 aromatics emitted from oil and gas production in this region (Warneke et al., 2014).  
98 Using the present dataset, we investigate diurnal variations, sources and sinks of nitrated  
99 phenols. We use a box model to analyze the budget of nitrated phenols in the atmosphere,  
100 and provide insights into the formation mechanism of nitrated phenols.

## 101 2. Measurements

102 The Uintah Basin Winter Ozone Study (UBWOS 2014) was conducted in January  
103 and February of 2014 at the Horse Pool site in the Uintah Basin, where over 10,000  
104 active oil and gas wells are located.

### 105 2.1 Acetate ToF-CIMS

#### 106 2.1.1, Instrument operation

107 An Aerodyne time-of-flight (ToF) CIMS (Lee et al., 2014) that uses acetate  
108 ( $\text{CH}_3\text{C}(\text{O})\text{O}^-$ ) as the reagent ion was deployed at the Horse Pool site during the UBWOS  
109 2014 to measure organic acids, inorganic acids and nitrated phenols. These compounds  
110 are ionized in the ion-molecule reaction region (IMR,  $61.8 \pm 0.3$  mbar) via proton  
111 abstraction (Veres et al., 2008) or by a sequence of clustering-declustering/deprotonation  
112 reactions (Brophy and Farmer, 2015) in the reaction with acetate ions. Acetate ions were  
113 produced by introducing saturated acetic anhydride/ $\text{N}_2$  mixture (5 mL/min) mixed with  
114 another flow of  $\text{N}_2$  (2.5 L/min) into a polonium-210 ( $^{210}\text{Po}$ ) radioactive source. The  
115 instrument was operated at strong de-clustering conditions by applying voltages in the  
116 first quadruple ion guide (i.e. SSQ,  $2.50 \pm 0.01$  mbar) during UBWOS 2014, with the ratio  
117 of acetate cluster ( $\text{CH}_3\text{C}(\text{O})\text{O}^- \cdot \text{CH}_3\text{C}(\text{O})\text{OH}$ )/acetate ( $\text{CH}_3\text{C}(\text{O})\text{O}^-$ ) at  $0.4\% \pm 0.1\%$ . Under  
118 such de-clustering conditions, the conjugate anions were usually observed as the product  
119 ions, with little contribution from cluster ions. The reagent ions and product ions are  
120 analyzed using a high-resolution time of flight mass spectrometer (TOFWERK,  
121 Switzerland). The signal of acetate ion was approximately  $1-2 \times 10^6$  count per second  
122 (cps) during the campaign (ToF extraction frequency=25 kHz). The mass resolution for  
123 the ToF during UBWOS 2014 was approximately 3200 for ions of  $m/z > 200$ .

Bin Yuan 12/27/2015 4:20 PM

Deleted:

125 Background signals associated with the instrument were measured every 2 hours  
126 for 15 min by passing ambient air through three stages of zero air generation: a platinum  
127 catalytic converter heated to 350 °C, nylon wool coated with sodium bicarbonate  
128 (NaHCO<sub>3</sub>), and activated charcoal, which were used in series to remove acidic gases  
129 from the sample air and determine instrument backgrounds. During the UBWOS 2014  
130 study, two CIMS inlets constructed from Teflon heated to ~40 °C with similar lengths  
131 (~10 m) placed at heights of 1 m and 18.5 m above ground were switched automatically  
132 every 30 min during the period of January 24- February 1, to measure the vertical  
133 concentration gradient of nitrated phenols and other acidic gases. Inlet switching between  
134 a long-heated and a short-unheated inlet was also conducted during February 1-5, to  
135 explore possible inlet interferences to CIMS measurements of nitrated phenols from the  
136 long-heated inlet. We did not observe differences in signals between the long and short  
137 inlets for nitrated phenols except DNP (Figure S1), indicating that potential loss in  
138 sampling line was minimal for the reported single nitrated phenols in this study. The inlet  
139 issues for DNP will be discussed in Section 2.1.2.

#### 140 2.1.2 Data processing

141 The ToF-CIMS data was processed using the TOFware software package  
142 ([www.tofwerk.com/tofware](http://www.tofwerk.com/tofware)) written in Igor Pro (Wavemetrics Inc., USA). The detailed  
143 data processing procedures are presented in recent studies (Yatavelli et al., 2014; Stark et  
144 al., 2015). Post-measurement mass calibrations were performed using nine isolated ions,  
145 including m/z 31.9904 (O<sub>2</sub><sup>-</sup>), m/z 34.9694 (Cl<sup>-</sup>), m/z 44.9982 (CHO<sub>2</sub><sup>-</sup>), m/z 59.0139  
146 (C<sub>2</sub>H<sub>3</sub>O<sub>2</sub><sup>-</sup>), m/z 61.9884 (NO<sub>3</sub><sup>-</sup>), m/z 143.9840 (C<sub>3</sub>F<sub>4</sub>O<sub>2</sub><sup>-</sup>), m/z 162.9824 (C<sub>3</sub>F<sub>5</sub>O<sub>2</sub><sup>-</sup>), m/z  
147 193.9808 (C<sub>4</sub>F<sub>6</sub>O<sub>2</sub><sup>-</sup>) and m/z 243.9776 (C<sub>5</sub>F<sub>8</sub>O<sub>2</sub><sup>-</sup>). The four fluorine-containing ions in the  
148 list were released from Teflon inlet during UBWOS 2014 and their persistent presence  
149 was used for mass calibration. The accuracy of mass calibration was 4.7±1.9 ppm for the  
150 whole campaign and the errors of mass calibration for individual ions were usually within  
151 10 ppm (average+3σ). The fitted raw signals for the targeted compounds were  
152 normalized using an acetate signal at the level of 1×10<sup>6</sup> cps.

153 The fitted m/z used for quantification of concentrations of nitrated phenols in the  
154 acetate CIMS are m/z 138.0197 (C<sub>6</sub>H<sub>4</sub>NO<sub>3</sub><sup>-</sup>) for NP, m/z 152.0353 (C<sub>7</sub>H<sub>6</sub>NO<sub>3</sub><sup>-</sup>) for MNP,

Bin Yuan 12/29/2015 1:14 PM

Deleted: 3.3

Bin Yuan 12/27/2015 4:21 PM

Deleted: .

Bin Yuan 12/27/2015 4:38 PM

Deleted: <https://sites.google.com/site/citofims/analysis-software/tofware>

Bin Yuan 12/27/2015 5:10 PM

Deleted:



160 m/z 166.0510 ( $C_8H_8NO_3^-$ ) for dimethylnitrophenol+ ethylnitrophenol (DMNP) and m/z  
161 183.0047 ( $C_6H_3N_2O_5^-$ ) for DNP. Compounds with same molecular formulas as nitrated  
162 phenols include phenyl nitrates/benzyl nitrates, methoxynitrobenzenes, nitrobenzyl  
163 alcohols and hydroxycarboxylic acids derived from pyridine. The first three groups of  
164 compounds have lower acidities than acetic acid (Bartmess, 2015) and hence they are  
165 unlikely to be observed in acetate CIMS, while hydroxycarboxylic acids derived from  
166 pyridine are expected to be small in the atmosphere.

167 High-resolution (HR) peak fitting to m/z 138, m/z 152 and m/z 183 in the averaged  
168 mass spectra of ToF-CIMS on a typical day (January 25, 2014) are shown as examples in  
169 Figure 2. Isotope signals from lower masses (dark green lines) accounted for small  
170 fractions of the m/z signals. Multiple overlapping ion peaks were identified in the m/z  
171 channels. In addition to nitrated phenols, several ions without deprotonation were also  
172 present in the even m/z (e.g.  $C_8H_{10}O_2^-$  at m/z 138), possibly due to electron transfer  
173 reactions and/or fragmentation in the quadrupole ion guides (Stark et al., 2015). The  
174 signals of NP and MNP were either the largest or significant larger than their neighboring  
175 peaks at their respective m/z, whereas the signal of DNP was much smaller than its  
176 neighboring peaks on January 25, 2014. Smaller ratios of the signals between the targeted  
177 peak and its neighboring peaks have been shown to deteriorate the precision of fitted  
178 signals for the targeted peak (Cubison and Jimenez, 2015; Müller et al., 2011; Corbin et al.,  
179 2015). Based on the provided equations in Cubison and Jimenez (2015), the imprecision  
180 arising from mass calibration (not including counting error) for the signals of NP, MNP  
181 and DNP are 3.2%, 1.8% and 47% based on the mass spectra of January 25, respectively.  
182 Imperfect mass calibration can also affect fitted magnitudes of ion signals. Figure S2  
183 shows the sensitivity of the fitted signals of various masses as a function of the errors in  
184 mass calibration. The signal changes at a 10 ppm (average+3 $\sigma$ ) error of mass calibration  
185 relative to perfect mass calibration (error=0 ppm) for NP, MNP and DNP signals are as  
186 high as 14%, 5% and 81%, respectively. The results from both precision calculation and  
187 sensitivity of fitted magnitudes indicate that the peak signals of NP and MNP can be  
188 fitted well with low uncertainties. The peak fitting at m/z 166 for DMNP shows similar  
189 results as m/z 138 for NP and m/z 152 for MNP. However, large uncertainties are  
190 associated with the peak signals of DNP on January 25, 2014, which is mainly affected

Bin Yuan 12/29/2015 3:20 PM

**Deleted:** Some examples of h

Bin Yuan 12/29/2015 3:21 PM

**Deleted:** the m/z

Bin Yuan 12/29/2015 3:21 PM

**Deleted:** the

Bin Yuan 12/27/2015 3:57 PM

**Deleted:** S

195 by the  $C_3F_6HO_2^-$  ions ( $m/z$  182.9886) as indicated by the opposite behaviors of the DNP  
196 ion and  $C_3F_6HO_2^-$  ion in Figure S2C.

197 The  $C_3F_6HO_2^-$  ion ( $m/z$  182.9886) was released from the heated Teflon inlet along  
198 with other fluorine-containing ions that were used for mass calibration. The release of  
199  $C_3F_6HO_2^-$  ion was supported by much higher signals from the long-heated inlet compared  
200 to the short-unheated inlet, when inlet-switching experiments were conducted in February  
201 2-5 (Figure S1). Long-heated inlets were used for most of the time during UBWOS 2014  
202 (January 23- February 13), except during January 18-22, when a short-unheated inlet was  
203 used. The averaged mass spectra of  $m/z$  183 measured on January 18 is shown in Figure  
204 2D. Compared to the mass spectra on January 25,  $C_3F_6HO_2^-$  signals on January 18 were  
205 lower and the signals of DNP were larger than of  $C_3F_6HO_2^-$  ions. As a result, the  
206 uncertainty from peak fitting for the DNP ion was much lower on January 18 (Figure  
207 S2D). Thus, we will only use measured DNP data in the beginning of the campaign  
208 (January 18-22), when the long heated inlet was not connected to the acetate CIMS and  
209 no inlet switching was performed.

210 The response of the CIMS instrument for nitrated phenols, including 2-NP, 4-NP, 2-  
211 methyl-4-nitrophenol and 2,5-dinitrophenol, was calibrated using a Liquid Calibration  
212 Unit (LCU, IONICON Analytik). In the LCU, a water solution with known  
213 concentrations of the targeted compounds is nebulized and diluted by another gas stream  
214 at different flow rates to produce a gas standard at various concentrations (Kaser et al.,  
215 2013). The results of the calibrations to various nitrated phenols are shown in Table 1.  
216 The sensitivity of 4-NP in our instrument was determined to be higher than that of 2-NP  
217 by a factor of 2.1. A higher sensitivity of 4-NP in acetate CIMS was reported in Mohr et  
218 al. (2013), but in that study the difference was significantly larger at three orders of  
219 magnitude (Mohr et al., 2013). The different sensitivity ratios of 4-NP/2-NP can be  
220 caused by many different instrumental conditions between our instrument and that in  
221 Mohr et al. (2013), such as the amount of acetic anhydride introduced into instrument,  
222 IMR and SSQ pressures, and de-clustering settings in the quadrupole ion guides, all of  
223 which affect sensitivities of acetate CIMS significantly (Stark et al., 2012). The main  
224 reagent ions in IMR were shown to be acetic acid-acetate clusters rather than acetate  
225 (Bertram et al., 2011) and the cluster distributions in IMR may depend on operated

Bin Yuan 12/25/2015 5:09 PM

**Deleted:** between our instrument and that in  
Mohr et al. (2013)

228 pressure in IMR and the amount of acetic anhydride into the ion source. While de-  
229 clustering in SSQ helps the interpretation of recorded mass spectra, de-clustering also  
230 obscures a precise understanding of cluster distributions in IMR and hence accurately  
231 prediction of sensitivities in acetate CIMS. This result also emphasizes the importance of  
232 instrument calibrations in deriving concentration from acetate CIMS. We note that 3-  
233 nitrophenol (3-NP) is not usually present in the atmosphere (Harrison et al., 2005a).  
234 Thus, the average of the sensitivities of 2-NP and 4-NP was used for calculating  
235 concentrations of NP. DMNP was not calibrated in this study and we assumed the same  
236 sensitivity as determined for MNP.

237 \_\_\_\_\_ The accuracies of nitrated phenols measurements by the CIMS are conservatively  
238 estimated to be around 40% for NP and 50% for other nitrated phenols, mainly arising  
239 from uncertainties in the concentrations output of the LCU (~10%), uncertainties  
240 associated with calibration procedures (~5%), errors in high-resolution (HR) [peak fittings](#)  
241 [to mass spectra \(see above and Figure S2\)](#), and the representativeness of the calibrated  
242 species to other isomers (0-30% for NP and 0-40% for other nitrated phenols). Assuming  
243 random errors in the observed ion counts follow a Poisson distribution, detection limits of  
244 nitrated phenols, i.e. concentrations with a signal to noise ratio (S/N) of 3, are calculated  
245 to be 0.1-0.3 ppt for 1-min average data (Table 1). Following the discussions in Bertram  
246 et al. (2011), the measured background ion counts in ToF-CIMS drift over time and thus  
247 detection limits are more appropriately calculated as the concentrations at three times of  
248 the standard deviation of the measurement background counts. The determined detection  
249 limits of nitrated phenols increase to the range of 0.3-0.5 ppt based on this approach  
250 (Bertram et al., 2011) (Table 1).

## 251 2.2 Other measurements

252 Volatile organic compounds (VOCs), including hydrocarbons and oxygenates, were  
253 measured using an online gas chromatography-mass spectrometer (GC-MS) (Gilman et  
254 al., 2013). A commercial proton transfer reaction time of flight mass spectrometer (PTR-  
255 TOF) (IONICON Analytik, Austria) was also deployed at the Horse Pool site to measure  
256 various VOC species (Warneke et al., 2015). Measurements of phenol, cresols and  
257 dimethylphenols+ethylphenols (DMP) were accomplished by the PTR-TOF at m/z

Bin Yuan 12/30/2015 1:21 PM

Deleted: fittings

Bin Yuan 12/29/2015 1:06 PM

Deleted: 0-10%

260 95.0491 ( $C_6H_6OH^+$ ),  $m/z$  109.0648 ( $C_7H_8OH^+$ ) and  $m/z$  123.0804 ( $C_8H_{10}OH^+$ ),  
261 respectively. [An example of high-resolution peak fitting to  \$m/z\$  95 in the mass spectra of](#)  
262 [PTR-TOF is shown in Figure S3](#). The sensitivities to these phenols are estimated here  
263 from the calibrated sensitivities of  $m/z$  93.0699 (toluene),  $m/z$  107.0855 (C8-aromatics)  
264 and  $m/z$  121.1012 (C9-aromatics) and the ratio of proton-transfer rate coefficients ( $k$ ) of  
265 the phenols versus the aromatic hydrocarbons (Cappellin et al., 2012) (see details in the  
266 SI). Considering the uncertainties in the rate coefficients  $k$ , the accuracies of the  
267 determined concentrations of phenols can be up to 50% (de Gouw and Warneke, 2007).

268 Measurements of  $NO_3$  and  $N_2O_5$  were conducted by a cavity ring-down  
269 spectroscopy instrument (Dubé et al., 2006).  $NO_x$  ( $NO+NO_2$ ),  $NO_y$  and  $O_3$  were  
270 measured with another cavity ring-down spectroscopy instrument (Wild et al., 2014).  
271 Measurements of methane ( $CH_4$ ) and carbon dioxide ( $CO_2$ ) were performed with a  
272 commercial cavity ring-down spectrometry instrument (Picarro G2301). A pair of  
273 commercial spectral radiometers (Metcon Inc.) was used to measure photolysis  
274 frequencies of ozone and  $NO_2$ .

### 275 3. Results and Discussions

#### 276 3.1 Diurnal variations

277 Measured diurnal profiles of NP, MNP and DMNP during the UBWOS 2014 are  
278 shown in Figure 3. Very strong diurnal variations in concentrations of these nitrated  
279 phenols were observed. Concentrations of nitrated phenols were higher at night and lower  
280 in the daytime. The ratios between the concentrations in the two hours around midnight  
281 (23:00-1:00 [MST](#)) and in the two hours around noon (11:00-13:00 [MST](#)) are 2.9, 3.9 and  
282 4.7 for NP, MNP and DMNP, respectively. This indicates that the substituted alkyl  
283 groups enhance the diurnal variations of nitrated phenols, either through larger source at  
284 night or larger sink in the daytime.

285 Primary emissions of VOCs and  $NO_x$  at the Horse Pool site are predominantly due  
286 to oil and gas production activities, as the Horse Pool site is surrounded by oil and gas  
287 production wells. VOCs and  $NO_x$  emitted from nearby oil and gas wells led to periodic  
288 concentration spikes during the UBWOS campaigns (Warneke et al., 2014; Yuan et al.,  
289 2015). Figure 4 shows two types of episodes encountered during UBWOS 2014. The first

Bin Yuan 12/27/2015 3:47 PM  
Deleted: 2

Bin Yuan 12/27/2015 3:47 PM  
Deleted: 3

292 was associated with high concentrations of methane and benzene, as an example of  
293 fugitive emissions from oil and gas wells. No enhancement of nitrated phenols was  
294 observed for the first emission episode. The second episode was associated with high  
295 concentrations of  $\text{NO}_y$ ,  $\text{NO}_x$  and  $\text{CO}_2$ , as an example of either vehicle emissions or other  
296 fuel combustion activities related to oil and gas extractions (e.g., compressors,  
297 dehydrators and pump jacks). High  $\text{NO}_x/\text{NO}_y$  ratios ( $0.96\pm 0.01$ ) indicate that a fresh  
298 combustion plume was encountered. We observed small enhancement of NP during the  
299 second emission episode. The enhancement ratio of NP/ $\text{NO}_y$  in this plume is determined  
300 to be  $4.6\pm 0.7\times 10^{-3}$  ppt/ppb, which is comparable with the reported NP/ $\text{NO}_x$  emission  
301 ratios ( $1\text{-}50\times 10^{-3}$  ppt/ppb) from gasoline and diesel vehicles (Inomata et al.,  
302 2013; Sekimoto et al., 2013). Using the obtained enhancement ratio of NP/ $\text{NO}_y$ , we  
303 determine that primary emissions from combustion sources only account for less than 2%  
304 of NP concentrations during UBWOS 2014. In addition to these primary sources,  
305 biomass burning was not observed in the UBWOS campaigns, based on the absence of  
306 any enhancement of biomass burning markers like acetonitrile. We conclude that primary  
307 emissions of nitrated phenols were not significant during UBWOS 2014.

308 In addition to primary emissions, secondary formation from oxidation of phenols is  
309 an important source for nitrated phenols (Harrison et al., 2005a). Phenol exhibited a  
310 concentration maximum in the afternoon (Figure 3B). The diurnal profile of phenol is  
311 more similar to that of secondary acetaldehyde, than that of primary emitted benzene. It  
312 suggests that secondary formation was the most important source of phenol. Substituted  
313 phenols (cresols and DMP) also had similar diurnal variations as phenol.

### 314 3.2 Modeling analysis for NP

#### 315 3.2.1 Box model results

316 We will focus on NP to understand the budget of nitrated phenols, because NP had  
317 higher concentrations than the substituted nitrated phenols (MNP and DMNP) and there  
318 is more information on sources and sinks of NP in the literature. A series of zero-  
319 dimensional box model simulations on the formation of phenol and NP were conducted  
320 using the online AtChem tool (<https://atchem.leeds.ac.uk>). The MCM v3.2 (Jenkin et al.,  
321 2012) was used as the chemical mechanism in the box model. We note that ambient

Bin Yuan 12/27/2015 3:47 PM

Deleted: 2B

323 temperature ( $-5\pm 5$  °C) during UBWOS 2014 was much lower than the temperature  
324 (around 25 °C) at which rate constants of many reactions are usually measured. Rate  
325 constants as a function of temperature are only available for the reactions of OH radical  
326 with benzene and phenol among those shown in Figure 1 and they were already included  
327 in MCM v3.2. The model ran in a time-dependent mode and a 48-hour spin-up time was  
328 applied in the box model. Measured concentrations of various hydrocarbons,  $\text{NO}_x$ ,  $\text{O}_3$ ,  
329  $\text{NO}_3$  and photolysis frequencies (Table S2) were used as constraints in the box model.  
330 The simulation period of the model was chosen to be January 18-27, a period associated  
331 with several buildup episodes of ozone and other secondary products, with high measured  
332 concentrations of NP and without precipitation. Following previous box model studies  
333 (Yuan et al., 2015; Edwards et al., 2014), dilution and deposition processes were  
334 represented together using a diurnally varying first-order physical loss parameter in the  
335 box model. The physical loss rate at night ( $5.8\times 10^{-6}$  s<sup>-1</sup>) was calculated from the decrease  
336 rate of NP concentration between 0:00-6:00 am when the chemical loss was expected to  
337 be low (see section 3.3.4). A higher physical loss rate ( $2.0\times 10^{-5}$  s<sup>-1</sup>) during daytime was  
338 used to account for larger turbulent mixing during daytime (Edwards et al., 2014), which  
339 results in the decrease of concentrations of inert tracers in the afternoon, e.g. benzene  
340 (Figure 3) and methane. Based on sensitivity tests of the box model, increase and  
341 decrease of the physical loss rate terms by a factor of two resulted in a -48% and +39% of  
342 change in the modeled NP concentrations.

343 As shown in the introduction, photolysis has been recognized as an important sink  
344 for nitrated phenols. However, the photolysis of NP (and other nitrated phenols) is not  
345 included in the MCM v3.2. We added the photolysis frequency of NP from Bardini  
346 (2006) (1.4% of photolysis frequency of  $\text{NO}_2$ ) into the MCM v3.2 and this model run is  
347 referred to as the base simulation. Here, we assume that photolysis of NP produces 2-  
348 phenoxy biradicals and HONO, as proposed in Bejan et al. (2006) (Figure 1 Route1).  
349 There are other possible chemical routes for photolysis of NP: producing phenoxy  
350 radicals ( $\text{C}_6\text{H}_5\text{O}$ ) by losing  $\text{NO}_2$  (Route2 in Figure 1) and producing nitrophenoxy radical  
351 by hydrogen abstraction (Route3 in Figure 1). The simulation test in Figure S4 indicates  
352 that the pathway forming  $\text{C}_6\text{H}_5\text{O}$  radicals and  $\text{NO}_2$  is an ineffective sink for NP, since  
353  $\text{C}_6\text{H}_5\text{O}$  radical will re-form NP by reacting with  $\text{NO}_2$ . However, we cannot exclude this

Bin Yuan 12/30/2015 1:46 PM

Deleted: N

Bin Yuan 12/25/2015 5:11 PM

Deleted: ial

Bin Yuan 12/27/2015 3:47 PM

Deleted: 2

Bin Yuan 12/27/2015 3:59 PM

Deleted: S3

Bin Yuan 12/25/2015 8:39 PM

Deleted: excludes

Bin Yuan 12/25/2015 8:40 PM

Deleted: phenoxy

Bin Yuan 12/25/2015 8:40 PM

Deleted: ( $\text{C}_6\text{H}_5\text{O}$ )

Bin Yuan 12/25/2015 8:40 PM

Deleted: as the main product from photolysis of NP

Bin Yuan 12/25/2015 8:41 PM

Deleted: and it would make photolysis an ineffective sink for NP

365 [pathway to occur along with that producing 2-phenoxy biradicals and HONO. The](#)  
366 [photolysis frequency determined in Bardini \(2006\) from concentration changes of 2-](#)  
367 [nitrophenol in a chamber may not include this pathway as well. As a result, attributing](#)  
368 [the photolysis rates determined in Bardini \(2006\) to other pathways other than Route2 is](#)  
369 [reasonable.](#) The route producing nitrophenoxy radical will be discussed in Section 3.3.

370 The simulated results for phenol and NP from the base case of the box model are  
371 shown in Figure [5](#). The modeled diurnal variations agreed reasonably well with the  
372 observation for both NP and phenol in the base simulation, except for the phenol  
373 nighttime levels that will be discussed below. Although modeled NP concentrations are  
374 higher than the measurements for both daytime and nighttime, the agreement between  
375 measurements and model results is still within their combined uncertainties.

376 The average measured concentrations of phenol at night are higher than 10 ppt, but  
377 the modeled phenol concentrations are usually less than 2 ppt. At night, the production of  
378 phenol from benzene oxidation halts, and the fast reaction with NO<sub>3</sub> ( $2.8 \times 10^{-11} \text{ cm}^3$   
379  $\text{molecule}^{-1} \text{ s}^{-1}$  at 298 K) removes phenol quickly (Figure [7](#) and discussion in section  
380 3.2.3). Measured nighttime NO<sub>3</sub> radicals were quite low during UBWOS 2014 ( $1.4 \pm 2.4$   
381 ppt). As a check on the possible uncertainties in measurements of NO<sub>3</sub> at these low  
382 levels, simulations by varying NO<sub>3</sub> concentrations by a factor of 2 result in little  
383 improvement for the modeled concentrations of phenol (Figure [S5](#)). Another simulation  
384 using calculated NO<sub>3</sub> concentrations from the equilibrium between NO<sub>3</sub> and N<sub>2</sub>O<sub>5</sub>  
385 (Figure [S5](#)) also indicates that uncertainties in NO<sub>3</sub> measurements cannot account for the  
386 discrepancies between measured and modeled phenol at night. The high phenol  
387 concentrations measured at night might be a result of primary emissions. Indeed, the  
388 measured phenol concentration was slightly enhanced in the plume with high methane  
389 concentrations (see Figure [4A](#)). However, a simulation using the measured phenol  
390 concentrations as a constraint in the box model, predicted much higher NP concentrations  
391 than measurements (Figure [S4](#)). Perhaps a more likely explanation for the enhanced  
392 phenol concentrations at night is that the measurements of phenol by PTR-TOF suffer  
393 from chemical interferences at night. Vinylfuran might be a candidate (Karl et al.,  
394 2007; Stockwell et al., 2015). Thus, the modeled concentrations of phenol shown in  
395 Figure [5](#) will be used in the following discussions.

Bin Yuan 12/27/2015 3:48 PM  
Deleted: 4

Bin Yuan 12/27/2015 3:49 PM  
Deleted: 6

Bin Yuan 12/27/2015 4:00 PM  
Deleted: S4

Bin Yuan 12/27/2015 4:00 PM  
Deleted: S4

Bin Yuan 12/27/2015 3:49 PM  
Deleted: 3A

Bin Yuan 12/27/2015 4:00 PM  
Deleted: S3

Bin Yuan 12/27/2015 3:49 PM  
Deleted: 4

### 403 3.2.2 NO<sub>2</sub> dependence of NP yields

404 As shown in Figure 1, NP is generated from the reaction of NO<sub>2</sub> with phenoxy  
405 radicals (C<sub>6</sub>H<sub>5</sub>O·) (Berndt and Boge, 2003), which is an intermediate from the reactions  
406 of OH and NO<sub>3</sub> radicals with phenol and the reaction of phenylperoxy radicals (C<sub>6</sub>H<sub>5</sub>O<sub>2</sub>)  
407 with NO. In addition to NO<sub>2</sub>, C<sub>6</sub>H<sub>5</sub>O· radicals also react with NO and O<sub>3</sub> (Platz et al.,  
408 1998) (see Figure 1), thus the yield of NP has been reported to depend on NO<sub>2</sub>  
409 concentrations in the atmosphere (Berndt and Boge, 2003).

410 In the MCM v3.2, only the reactions of C<sub>6</sub>H<sub>5</sub>O radical with O<sub>3</sub> and NO<sub>2</sub> are  
411 included and here we added the reaction of C<sub>6</sub>H<sub>5</sub>O with NO ( $k=1.88\times 10^{-12}$  cm<sup>3</sup> molecule<sup>-1</sup>  
412 s<sup>-1</sup>) for a new simulation. Compared to the base simulation, the modeled concentrations  
413 of NP are lower, especially for the period of 11:00-17:00, as the effective yield of NP is  
414 reduced (Figure 5). The small enhancement during the period of 11:00-17:00 in NP  
415 concentrations from the base simulation is absent in the simulation with the reaction of  
416 C<sub>6</sub>H<sub>5</sub>O with NO. The variations of modeled NP concentrations in the daytime from the  
417 new simulation are in better agreement with the measurements (Figure 5). This indicates  
418 the reaction of NO and C<sub>6</sub>H<sub>5</sub>O radical should be considered to account for the NO<sub>2</sub>  
419 dependence of NP formation.

420 Another simulation using fixed NP yields from phenol oxidation reported in  
421 Atkinson et al. (1992) (6.7% for OH oxidation and 25.1% for NO<sub>3</sub> oxidation) is also  
422 performed. This simulation neglects any dependence of NP yield from phenol oxidation  
423 on concentrations of NO<sub>2</sub>, O<sub>3</sub> and NO. We observed lower concentrations during both the  
424 day and night compared to the base simulation (Figure 5). However, the enhancement of  
425 modeled NP in the period of 11:00 -17:00 is distinctly observed with the simulation using  
426 the fixed yields in Atkinson et al. (1992), which is in contrast to the lowest concentration  
427 in the afternoon from our observations. This, again, indicates there must be a dependence  
428 of NP yield from phenol oxidation on NO<sub>2</sub> concentrations in the atmosphere.

### 429 3.2.3 Gas-particle partitioning of NP

430 NP formed in the gas phase can partition into particles (Harrison et al., 2005a).  
431 Measurements in several studies demonstrated that 2-NP and MNP were mainly found in  
432 the gas phase (Herterich and Herrmann, 1990; Cecinato et al., 2005; Morville et al., 2006).

Bin Yuan 12/27/2015 3:49 PM

Deleted: 4

Bin Yuan 12/27/2015 3:49 PM

Deleted: 4

Bin Yuan 12/27/2015 3:49 PM

Deleted: 4



436 However, the reported particle fractions of 4-NP and DNP exhibit a broad range in  
437 values: the particle fractions of 4-NP and DNP reported in Herterich and Herrmann  
438 (1990) were both lower than 15%, whereas most of the concentrations of 4-NP (>75%)  
439 (Cecinato et al., 2005) and DNP (>95%) (Morville et al., 2006) were detected in particles  
440 in these other two studies.

441 The concentrations of NP and other nitrated phenols in particles were not measured  
442 in this study. We acknowledge that some fractions of nitrated phenols in particles may  
443 evaporate into gas phase in the heated inlets. If it holds true, the measured concentrations  
444 of nitrated phenols in this study would fall somewhere between concentrations in gas-  
445 phase and the total gas+particle concentrations. Here, the gas-particle partitioning of NP  
446 as a function of time was estimated using the equilibrium absorption partitioning theory  
447 (Pankow, 1994; Donahue et al., 2006) (see details in the SI), based upon pure compound  
448 liquid vapor pressure of 2-NP and 4-NP (Schwarzenbach et al., 1988) (Table 2) and  
449 measured organic aerosol (OA) concentrations with an aerosol mass spectrometer  
450 (AMS). The dependence with temperature was accounted for using the Clausius-  
451 Clapeyron relationship with reported enthalpies of evaporation ( $H_{\text{vap}}$ ) (Schwarzenbach et  
452 al., 1988). Although vapor pressures from Schwarzenbach et al. (1988) might have  
453 significant uncertainties, Schwarzenbach et al. (1988) provided the only comprehensive  
454 measurements of sub-cooled liquid vapor pressures of nitrated phenols reported in the  
455 literature.

456 The calculated fractions in particle ( $F_p$ ) for 2-NP were generally very low (campaign  
457 average:  $1.1 \pm 0.9 \times 10^{-4}$ , max:  $7.3 \times 10^{-4}$ ), whereas  $F_p$  for 4-NP were higher (average:  
458  $0.053 \pm 0.048$ , max: 0.38). The variability of the determined  $F_p$  values is the result of  
459 variations of both OA concentrations ( $12.5 \pm 8.7 \mu\text{g}/\text{m}^3$ , min:  $<1 \mu\text{g}/\text{m}^3$ , max:  $42.6 \mu\text{g}/\text{m}^3$ )  
460 and ambient temperature ( $-5 \pm 5 \text{ }^\circ\text{C}$ , min:  $-17 \text{ }^\circ\text{C}$ , max:  $10 \text{ }^\circ\text{C}$ ) during the campaign. The  
461 higher  $F_p$  for 4-NP is expected, as 4-NP ( $1.4 \times 10^{-3}$  Torr at 298 K) has much lower vapor  
462 pressure than 2-NP (0.20 Torr at 298 K) (Table 2). In addition to absorption, partitioning  
463 of NP into aqueous phase of particles is another possible pathway affecting  $F_p$ . This  
464 mechanism is estimated using Henry's law constants (Sander, 2015) and determined  
465 liquid water content (LWC) ( $8.4 \pm 7.5 \mu\text{g}/\text{m}^3$ ) in aerosol using the ISORROPIA model  
466 (Fountoukis and Nenes, 2007). The estimated  $F_p$  values based on aqueous phase

Bin Yuan 12/29/2015 3:58 PM

Deleted:

Bin Yuan 12/30/2015 1:22 PM

Deleted: as

469 partitioning for 2-NP ( $1.3 \times 10^{-7}$ ) and 4-NP ( $3.0 \times 10^{-5}$ ) are both much lower than  $F_p$   
 470 | estimated from the **equilibrium** absorption partitioning theory, indicating partitioning of  
 471 NP into particle aqueous phase was not important during UBWOS 2014.

472 The gas-particle partitioning of 2-NP and 4-NP determined above was incorporated  
 473 into the box model by constraining the estimated  $F_p$  in the determination of gas-particle  
 474 mass transport rates. The mass transport rates ( $R_{in}$  and  $R_{out}$ ) of a species into and out of  
 475 particles with radius  $r$  are approximated by (Jacob, 2000):

$$R_{in} = \left( \frac{r}{D_g} + \frac{4}{v\alpha} \right)^{-1} A \times c_g = \frac{1}{\tau} \times c_g \quad (1)$$

$$R_{out} = \left( \frac{r}{D_g} + \frac{4}{v\alpha} \right)^{-1} A \times \frac{c_p}{K_{ep}} = \frac{1}{\tau} \times \frac{c_p}{K_{ep}} \quad (2)$$

476 where  $c_g$  and  $c_p$  are concentrations of the species in the gas and particle phase.  $D_g$   
 477 is the gas-phase molecular diffusion coefficient ( $\text{m}^2 \text{s}^{-1}$ ),  $v$  is the mean molecular speed  
 478 ( $\text{m s}^{-1}$ ),  $\alpha$  is the mass accommodation coefficient.  $A$  is the aerosol surface area per unit  
 479 | volume of air ( $\text{m}^2 \text{m}^{-3}$ ).  $K_{ep}$  is the equilibrium constant, i.e.  $c_p/c_g$ , or  $F_p/(1 - F_p)$ . The  
 480 characteristic time scale of mass transfer ( $\tau$ ) is estimated to be on the order of minutes for  
 481 particles in the troposphere (Bowman et al., 1997; Jacob, 2000). Thus, rather than  
 482 determining the characteristic time scale explicitly, we assume that the equilibrium is  
 483 maintained at each model step ( $\tau=5$  min). After entering into particles, no further reaction  
 484 of NP was prescribed in the model. The modeled diurnal profiles of NP associated with  
 485 | the inclusion of gas-particle partitioning are shown in Figure 6. Compared to the base  
 486 simulation, the modeled NP concentrations in the gas phase using the estimated  $F_p$  from  
 487 4-NP are lower (4-8%) for most of the day and slightly higher (2-3%) in the morning  
 488 when NP concentrations decreased quickly. Since the predicted  $F_p$  from 2-NP is very  
 489 small, the modeled NP concentrations in the gas phase using the estimates from 2-NP  
 490 were almost identical to the base simulation. In contrast with the modeled concentrations  
 491 of NP in the gas phase, the modeled total concentrations of NP in gas and particle phase  
 492 are consistently higher than the base simulation that do not consider gas-particle  
 493 partitioning. In summary, we observe relatively small changes of the modeled gaseous  
 494 NP concentrations after the inclusion of gas-particle partitioning in the box model.

Bin Yuan 10/26/2015 4:25 PM

Deleted:  $\frac{1-F_p}{F_p}$

Bin Yuan 12/27/2015 3:49 PM

Deleted: 5

497 Further measurements of the gas/particle partitioning of nitrated phenols are needed to  
498 explain the variety of  $F_p$  values observed in different studies and/or the potential  
499 differences between measurements and prediction from the equilibrium absorption  
500 partitioning model.

### 501 3.2.4 Budget analysis of phenol and nitrophenol

502 Diurnal profiles of formation and loss rates derived from the base simulation of the  
503 box model for both phenol and NP are shown in Figure 7. Production of phenol only  
504 occurs in the daytime from OH oxidation of benzene. The magnitudes of losses of phenol  
505 due to OH oxidation (21 ppt/day) and  $\text{NO}_3$  oxidation (19 ppt/day) are comparable on a  
506 daily basis. From morning to afternoon (8:00-15:00), production of phenol is larger than  
507 the losses, resulting in continuous growth of phenol concentrations in this period. After  
508 15:00 pm, the losses start to surpass the production and phenol concentrations decrease  
509 quickly. With fast reduction of phenol concentrations in the evening, phenol loss from the  
510 reaction with  $\text{NO}_3$  is mainly occurred before midnight.

511 As shown in Figure 7, NP is produced during both daytime and night, with more  
512 production in the daytime. As mentioned earlier, the only formation pathway of NP is  
513 from the reaction of phenoxy radicals ( $\text{C}_6\text{H}_5\text{O}$ ) with  $\text{NO}_2$ , so the contribution from  
514 different pathways to NP formation can be derived from source analysis of  $\text{C}_6\text{H}_5\text{O}$   
515 radicals (Figure 7C). The production of  $\text{C}_6\text{H}_5\text{O}$  radicals is dominated by the reaction of  
516  $\text{C}_6\text{H}_5\text{O}_2$  radicals with NO during daytime (71% for 24-hour average) and the reaction of  
517 phenol with  $\text{NO}_3$  radicals at night (27% for 24-hour average). There are several sources  
518 contributing to the formation of  $\text{C}_6\text{H}_5\text{O}_2$  radicals in the MCM, including photolysis of  
519 benzaldehyde and peroxybenzoic acid, OH oxidation of benzoic acid and phenyl  
520 hydroperoxide, and degradations of other radicals (e.g., phenylperoxyacyl radical  
521  $\text{C}_6\text{H}_5\text{CO}_3$ ), suggesting a wide range of aromatic compounds as the precursors of NP in  
522 the daytime. The reaction of phenol with OH radicals only accounts for a small fraction  
523 of the production of  $\text{C}_6\text{H}_5\text{O}$  radicals (2% for 24-hour average), **due to the small yield of**  
524 **NP (6%) from the reaction of OH with phenol in the MCM. It indicates** phenol is not an  
525 important precursor for NP during daytime. The destruction of NP is mainly due to  
526 photolysis (17 ppt/day), with some contributions from  $\text{NO}_3$  reaction (1.7 ppt/day). The

Bin Yuan 12/27/2015 3:49 PM

Deleted: 6

Bin Yuan 12/27/2015 3:49 PM

Deleted: 6

Bin Yuan 12/27/2015 3:50 PM

Deleted: 6C

Bin Yuan 12/25/2015 9:59 PM

Deleted: indicating

531 reaction with OH radicals is not important for the losses of NP in the UBWOS 2014.  
532 Dilution/deposition processes account for 20% of the total loss of NP in the box model.  
533 Our results are consistent with previous proposal on photolysis as the dominant chemical  
534 loss pathway for nitrated phenols (Bejan et al., 2007). Based on the conditions at the  
535 Horse Pool site, the lifetime of NP due to photolysis at noontime is calculated to be ~80  
536 min. As the result of the short lifetime of NP during daytime, the production (23.6  
537 ppt/day) and loss rates (23.1 ppt/day) of NP maintain a balanced budget of NP on a daily  
538 basis. The inclusion of the reaction of phenoxy radicals (C<sub>6</sub>H<sub>5</sub>O) with NO discussed in  
539 section 3.2.2 would mainly affect NP budget in the noontime, with smaller production  
540 and loss in this period.

541 The different diurnal variations of production and loss rates of NP explain the  
542 measured diurnal profile of NP concentrations shown in Figure 3. The increase of loss  
543 rates from photolysis result in the quick decline of NP concentrations in the morning. The  
544 formation of NP from NO<sub>3</sub> oxidation of phenol in the evening exceeds the destruction of  
545 NP, which accounts for the enhancement of NP in this period. The formation and loss  
546 rates of NP are comparable in the afternoon and relatively constant concentrations of NP  
547 were observed.

548 A previous study showed that photolysis of nitrated phenols contributes to HONO  
549 formation (Bejan et al., 2006). If we assume photolysis of nitrated phenols at rates of  
550 1.4%×J(NO<sub>2</sub>) yields HONO at a 100% yield (upper limit), photolysis of NP, MNP and  
551 DMNP together accounted for a formation rate of HONO of 1.5±1.9 ppt/hour around  
552 noontime (9:00-15:00) during UBWOS 2014. This photolysis source would increase the  
553 steady state concentrations of HONO by 0.5 ppt in early morning (7:00-8:30) and 0.2 ppt  
554 during the noontime period (9:00-15:00), which are only small fractions of measured  
555 HONO concentrations (50-100 ppt) during UBWOS 2014 (Edwards et al., 2014).

### 556 3.3 Dinitrophenol

557 Further oxidation of NP in the presence of NO<sub>x</sub> produces DNP. The measured time  
558 series of DNP in January 18-22 is shown in Figure 8. A similar diurnal profile was  
559 observed for DNP as other nitrated phenols, associated with higher concentrations at  
560 night and lower in the daytime. We also notice that the peak time of DNP concentrations

Bin Yuan 12/27/2015 3:50 PM

Deleted: 2

Bin Yuan 12/25/2015 10:33 PM

Deleted: a 100% yield of

Bin Yuan 12/25/2015 10:33 PM

Deleted: from photolysis of nitrated phenols

Bin Yuan 12/29/2015 1:10 PM

Deleted: Measurements of DNP using the acetate CIMS were challenging during UBWOS 2014, due to the influence of a fluorine ion (C<sub>3</sub>F<sub>6</sub>HO<sub>2</sub><sup>-</sup>, m/z 182.9886) released from the heated Teflon inlet (see Figure S2 for peak fitting example). The release of C<sub>3</sub>F<sub>6</sub>HO<sub>2</sub><sup>-</sup> ion was supported by much higher signals of this ion from the long-heated inlet compared to the short-unheated inlet, when inlet-switching experiments were conducted in February 2-5 (Figure S1). We also observed that several other fluorine ions were released from the heated inlet ions, such as C<sub>2</sub>F<sub>3</sub>O<sub>2</sub><sup>-</sup>, C<sub>3</sub>F<sub>4</sub>O<sub>2</sub><sup>-</sup> and C<sub>3</sub>F<sub>5</sub>O<sub>2</sub><sup>-</sup>. The presence of C<sub>3</sub>F<sub>6</sub>HO<sub>2</sub><sup>-</sup> ion made it difficult to get accurate signals of the ion for of DNP (m/z 183.0047) for most of the time during UBWOS 2014, when the long-heated inlet was used (Figure S1). As a result, we will only use measured DNP data in the beginning of the campaign (January 18-22), when the long heated inlet was not connected to the acetate CIMS and no inlet switching was performed. [1]

Bin Yuan 12/27/2015 3:50 PM

Deleted: 7

589 at night was somewhat later than NP, consistent with further oxidation of NP as the  
590 source of DNP.

591 In the MCM v3.2, reactions of NP with OH or NO<sub>3</sub> radicals generate nitrophenoxy  
592 radicals (NO<sub>2</sub>C<sub>6</sub>H<sub>5</sub>O·), which react further with NO<sub>2</sub> to form DNP. Here, we assume  
593 DNP has the same photolysis rate as NP (1.4% of photolysis frequency of NO<sub>2</sub>) (Bardini,  
594 2006) and we added the photolysis into the MCM v3.2. The simulated concentrations of  
595 DNP from the box model are also displayed in Figure 8. The agreement between  
596 measurements and simulation is quite good from the base simulation. DNP has also been  
597 observed in the particle phase at significant fractions (Morville et al., 2006). Using the  
598 equilibrium absorption partitioning theory described in section 3.3.3 and vapor pressures  
599 of two different DNP isomers (2,4-DNP and 2,5-DNP) (Table 2), we incorporated the  
600 calculated particle fractions of DNP (Table 2) into the box model as a sensitivity  
601 simulation. The predicted DNP concentrations from this simulation are around 5% lower  
602 than the base simulation at night. Considering the limited information on DNP formation,  
603 the agreement between measured and modeled concentrations of DNP from both  
604 simulations is encouraging. This degree of agreement implies that DNP concentrations  
605 measured in UBWOS 2014 is explainable by known chemical reactions in the gas phase.

606 As described in Section 3.2, photolysis is the dominant sink for NP and box  
607 model results indicate that photolysis of NP may not generate phenoxy radical (by losing  
608 NO<sub>2</sub>). The other possible product from photolysis of NP is nitrophenoxy radical (Figure 1  
609 Route 3), which would act as a secondary source of DNP. This assumption is evaluated  
610 as a new simulation. The simulation predicted concentration peaks of DNP in the  
611 morning (the orange line in Figure 8), which are not observed in our measurements.

612 Thus, we exclude nitrophenoxy radical as the main products of photolysis of NP.

613 However, the products and exact chemical mechanisms for photolysis of NP remain  
614 unclear and thus the photolysis of NP warrants further detailed studies.

### 615 3.4 Non-gas phase reactions

616 The box model only considers gas phase reactions that produce nitrated phenols. In  
617 addition to gas phase reactions, aqueous reactions in particles and heterogeneous  
618 reactions are other potential sources of nitrated phenols (Harrison et al., 2005a). As

Bin Yuan 12/27/2015 3:50 PM

Deleted: 7

Bin Yuan 12/30/2015 1:23 PM

Deleted: also

Bin Yuan 12/27/2015 3:50 PM

Deleted: 7

Bin Yuan 12/30/2015 1:23 PM

Deleted: Combining the results in section 3.2 and here

Bin Yuan 12/30/2015 1:23 PM

Deleted: both phenoxy radical and

625 | shown in section 3.3.3, using chemical compositions of aerosol at the Horse Pool site and  
626 | the ISORROPIA model (Fountoukis and Nenes, 2007), the liquid water content (LWC) in  
627 | aerosol during UBWOS 2014 was estimated to be  $8.4 \pm 7.5 \mu\text{g}/\text{m}^3$  (whole campaign  
628 | average), or  $8.4 \pm 7.5 \times 10^{-12}$  expressed as the volume fraction. Based on the box modeling  
629 | results in Harrison et al. (2005b), aqueous reactions contribute less than 2% of NP  
630 | production at  $3 \times 10^{-9}$  volume fraction LWC. Thus, aqueous reactions in UBWOS 2014  
631 | should not be a significant source for nitrated phenols compared to gas phase reactions.

632 | The Uintah Basin was covered by snow during UBWOS 2014. The importance of  
633 | heterogeneous reactions on snow surface to formation of nitrated phenols is evaluated  
634 | using measurements of the vertical gradients of these species. Here, the concentration  
635 | gradient is defined as the concentrations measured at 18.5 m subtracted from those  
636 | measured at 1 m. As shown in Figure 9, we observed negative concentration gradients for  
637 | nitrated phenols at night, indicating that deposition was playing a role and consequently  
638 | ground snow was a net sink for nitrated phenols at night. A previous study suggested  
639 | heterogeneous reaction of  $\text{N}_2\text{O}_5$  with phenol in the aqueous phase produces NP (Heal et  
640 | al., 2007). Strong deposition of  $\text{N}_2\text{O}_5$  to the snow surface was observed at night during  
641 | UBWOS 2014, but as discussed no production of nitrated phenols near the snow surface  
642 | was detected at night (Figure 9). The vertical gradients for nitrated phenols in the daytime  
643 | fluctuated around zero with large variations, which might be a result of their low  
644 | concentrations during daytime. The analysis of vertical gradients implies that  
645 | heterogeneous reactions on snow surface may not be important for formation of nitrated  
646 | phenols in the atmosphere during UBWOS 2014.

#### 647 | 4. Conclusions

648 | In this study, nitrated phenols in the gas phase were measured using an online  
649 | acetate ToF-CIMS in an oil and gas production region during winter. Strong diurnal  
650 | profiles were observed for nitrated phenols, with concentration maxima at night. As the  
651 | dominant sink for nitrated phenols, photolysis accounted for lower concentrations of  
652 | nitrated phenols during daytime. We determined that the photolysis of nitrated phenols  
653 | was not an important source of HONO during UBWOS 2014. Based on box model  
654 | results, NP was mainly formed in the daytime (73%) from a wide range of precursors,

Bin Yuan 12/30/2015 1:24 PM

Deleted: the

Bin Yuan 12/30/2015 1:24 PM

Deleted: here

Bin Yuan 12/27/2015 3:51 PM

Deleted: 8

Bin Yuan 12/27/2015 3:51 PM

Deleted: 8

659 with significant contribution from the reaction of phenol with NO<sub>3</sub> radicals at night  
660 (27%). Box model results also indicated that gas phase oxidation of aromatics was able to  
661 explain the measured concentrations of NP and DNP. We demonstrated that box model  
662 results provided valuable information on the detailed chemical mechanisms in the  
663 formation and destruction of NP, e.g., the NO<sub>2</sub> dependence of NP yields from phenol  
664 oxidations and chemical products of NP photolysis. We determined that aqueous-phase  
665 reactions and heterogeneous reactions were minor sources of nitrated phenols in this  
666 study. Although the dataset of nitrated phenols was collected in an oil and gas production  
667 region, the chemistry in secondary formation of nitrated phenols and the dynamics of the  
668 budget of nitrated phenols in other regions, e.g., urban areas, should behave similarly to  
669 those shown in this study.

670 Biomass burning activity did not affect the UBWOS 2014 measurements, and the  
671 concentrations of phenols and nitrated phenols were mainly from oxidations of aromatics  
672 in the atmosphere. The measurements during UBWOS 2014 provided a great opportunity  
673 to study secondary formation of nitrated phenols in the absence of other confounding  
674 sources. The UBWOS 2014 campaign also represented the first coincident and high time-  
675 resolution measurements of aromatic hydrocarbons, phenols and nitrated phenols in  
676 ambient air. The measurements of phenol and nitrated phenols provided a better  
677 understanding of their sources, budgets and roles in atmospheric chemistry and for the  
678 evaluation of the oxidation mechanisms of aromatics. This is achieved by the emergence  
679 of the new ToF-CIMS and PTR-TOF techniques. We envision that these techniques will  
680 provide the ability to detect many other intermediate compounds in the atmosphere and  
681 that the measurements will advance the understanding of atmospheric oxidation  
682 processes.

683

#### 684 **Acknowledgement**

685 The Uintah Basin Winter Ozone Studies were a joint project led and coordinated by the  
686 Utah Department of Environmental Quality (UDEQ) and supported by the Uintah Impact  
687 Mitigation Special Service District (UIMSSD), the Bureau of Land Management (BLM),  
688 the Environmental Protection Agency (EPA) and Utah State University. This work was

Bin Yuan 12/30/2015 1:24 PM

Deleted: the

690 funded in part by the Western Energy Alliance, and NOAA's Atmospheric Chemistry,  
691 Climate and Carbon Cycle program. We thank Questar Energy Products for site  
692 preparation and support. Chemical compositions of aerosol were provided by Tim Bates  
693 and James Johnson from NOAA Pacific Marine Environmental Laboratory (PMEL) and  
694 the Joint Institute for the Study of the Atmosphere and Ocean (JISAO) at University of  
695 Washington.  
696



697 **References:**

- 698 Atkinson, R., Aschmann, S. M., and Arey, J.: Reactions of hydroxyl and nitrogen trioxide  
699 radicals with phenol, cresols, and 2-nitrophenol at  $296 \pm 2$  K, *Environmental Science &*  
700 *Technology*, 26, 1397-1403, 10.1021/es00031a018, 1992.
- 701 Bardini, P.: *Atmospheric Chemistry of Dimethylphenols & Nitrophenols*, PhD,  
702 University College Cork, Corcaigh, 2006.
- 703 Bartmess, J. E.: Negative Ion Energetics Data, NIST Chemistry WebBook, NIST  
704 Standard Reference Database Number 69, edited by: Linstrom, P. J., and Mallard, W.  
705 G., National Institute of Standards and Technology, Gaithersburg MD, 20899  
706 <http://webbook.nist.gov>, (retrieved August 28, 2015). 2015.
- 707 Bejan, I., Abd El Aal, Y., Barnes, I., Benter, T., Bohn, B., Wiesen, P., and Kleffmann, J.:  
708 The photolysis of ortho-nitrophenols: a new gas phase source of HONO, *Phys Chem*  
709 *Chem Phys*, 8, 2028-2035, 2006.
- 710 Bejan, I., Barnes, I., Olariu, R., Zhou, S., Wiesen, P., and Benter, T.: Investigations on  
711 the gas-phase photolysis and OH radical kinetics of methyl-2-nitrophenols, *Phys Chem*  
712 *Chem Phys*, 9, 5686-5692, 10.1039/B709464G, 2007.
- 713 Bejan, I., Duncianu, M., Olariu, R., Barnes, I., Seakins, P. W., and Wiesen, P.: Kinetic  
714 Study of the Gas-Phase Reactions of Chlorine Atoms with 2-Chlorophenol, 2-  
715 Nitrophenol, and Four Methyl-2-nitrophenol Isomers, *The Journal of Physical*  
716 *Chemistry A*, 119, 4735-4745, 10.1021/acs.jpca.5b02392, 2015.
- 717 Berndt, T., and Boge, O.: Gas-phase reaction of OH radicals with phenol, *Phys Chem*  
718 *Chem Phys*, 5, 342-350, 10.1039/B208187C, 2003.
- 719 Bertram, T. H., Kimmel, J. R., Crisp, T. A., Ryder, O. S., Yatavelli, R. L. N., Thornton, J.  
720 A., Cubison, M. J., Gonin, M., and Worsnop, D. R.: A field-deployable, chemical  
721 ionization time-of-flight mass spectrometer, *Atmos. Meas. Tech.*, 4, 1471-1479,  
722 10.5194/amt-4-1471-2011, 2011.
- 723 Bolzacchini, E., Bruschi, M., Hjorth, J., Meinardi, S., Orlandi, M., Rindone, B., and  
724 Rosenbohm, E.: Gas-Phase Reaction of Phenol with NO<sub>3</sub>, *Environmental Science &*  
725 *Technology*, 35, 1791-1797, 10.1021/es001290m, 2001.
- 726 Bowman, F. M., Odum, J. R., Seinfeld, J. H., and Pandis, S. N.: Mathematical model for  
727 gas-particle partitioning of secondary organic aerosols, *Atmospheric Environment*, 31,  
728 3921-3931, [http://dx.doi.org/10.1016/S1352-2310\(97\)00245-8](http://dx.doi.org/10.1016/S1352-2310(97)00245-8), 1997.
- 729 Brophy, P., and Farmer, D. K.: A switchable reagent ion high resolution time-of-flight  
730 chemical ionization mass spectrometer for real-time measurement of gas phase  
731 oxidized species: characterization from the 2013 southern oxidant and aerosol study,  
732 *Atmospheric Measurement Techniques*, 8, 2945-2959, 10.5194/amt-8-2945-2015,  
733 2015.
- 734 Cappellin, L., Karl, T., Probst, M., Ismailova, O., Winkler, P. M., Soukoulis, C., Aprea,  
735 E., Mark, T. D., Gasperi, F., and Biasioli, F.: On quantitative determination of volatile  
736 organic compound concentrations using proton transfer reaction time-of-flight mass  
737 spectrometry, *Environ Sci Technol*, 46, 2283-2290, 10.1021/es203985t, 2012.
- 738 Caralp, F., Foucher, V., Lesclaux, R., J. Wallington, T., and D. Hurley, M.: Atmospheric  
739 chemistry of benzaldehyde: UV absorption spectrum and reaction kinetics and  
740 mechanisms of the C<sub>6</sub>H<sub>5</sub>C(O)O<sub>2</sub> radical, *Phys Chem Chem Phys*, 1, 3509-3517,  
741 10.1039/A903088C, 1999.

742 Cecinato, A., Di Palo, V., Pomata, D., Tomasi Scianò, M. C., and Possanzini, M.:  
743 Measurement of phase-distributed nitrophenols in Rome ambient air, *Chemosphere*, 59,  
744 679-683, <http://dx.doi.org/10.1016/j.chemosphere.2004.10.045>, 2005.

745 Chen, J., Wenger, J. C., and Venables, D. S.: Near-Ultraviolet Absorption Cross Sections  
746 of Nitrophenols and Their Potential Influence on Tropospheric Oxidation Capacity,  
747 *The Journal of Physical Chemistry A*, 115, 12235-12242, 10.1021/jp206929r, 2011.

748 Cheng, S.-B., Zhou, C.-H., Yin, H.-M., Sun, J.-L., and Han, K.-L.: OH produced from o-  
749 nitrophenol photolysis: A combined experimental and theoretical investigation, *The*  
750 *Journal of Chemical Physics*, 130, 234311,  
751 doi:<http://dx.doi.org/10.1063/1.3152635>, 2009.

752 Corbin, J., Othman, A., D. Allan, J., R. Worsnop, D., D. Haskins, J., Sierau, B.,  
753 Lohmann, U., and A. Mensah, A.: Peak-fitting and integration imprecision in the  
754 Aerodyne aerosol mass spectrometer: effects of mass accuracy on location-constrained  
755 fits, *Atmospheric Measurement Techniques*, 8, 4615-4636, 10.5194/amt-8-4615-2015,  
756 2015.

757 Cubison, M. J., and Jimenez, J. L.: Statistical precision of the intensities retrieved from  
758 constrained fitting of overlapping peaks in high-resolution mass spectra, *Atmospheric*  
759 *Measurement Techniques*, 8, 2333-2345, 10.5194/amt-8-2333-2015, 2015.

760 de Gouw, J., and Warneke, C.: Measurements of volatile organic compounds in the  
761 earth's atmosphere using proton-transfer-reaction mass spectrometry, *Mass*  
762 *Spectrometry Reviews*, 26, 223-257, 2007.

763 Delhomme, O., Morville, S., and Millet, M.: Seasonal and diurnal variations of  
764 atmospheric concentrations of phenols and nitrophenols measured in the Strasbourg  
765 area, France, *Atmospheric Pollution Research*, 16-22, 10.5094/APR.2010.003, 2010.

766 Desyaterik, Y., Sun, Y., Shen, X., Lee, T., Wang, X., Wang, T., and Collett, J. L.:  
767 Speciation of "brown" carbon in cloud water impacted by agricultural biomass burning  
768 in eastern China, *Journal of Geophysical Research: Atmospheres*, 118, 7389-7399,  
769 10.1002/jgrd.50561, 2013.

770 Donahue, N. M., Robinson, A. L., Stanier, C. O., and Pandis, S. N.: Coupled Partitioning,  
771 Dilution, and Chemical Aging of Semivolatile Organics, *Environmental Science &*  
772 *Technology*, 40, 2635-2643, 10.1021/es052297c, 2006.

773 Dubé, W. P., Brown, S. S., Osthoff, H. D., Nunley, M. R., Ciciora, S. J., Paris, M. W.,  
774 McLaughlin, R. J., and Ravishankara, A. R.: Aircraft instrument for simultaneous, in  
775 situ measurement of NO<sub>3</sub> and N<sub>2</sub>O<sub>5</sub> via pulsed cavity ring-down spectroscopy, *Review*  
776 *of Scientific Instruments*, 77, 034101, doi:<http://dx.doi.org/10.1063/1.2176058>,  
777 2006.

778 Edwards, P. M., Brown, S. S., Roberts, J. M., Ahmadov, R., Banta, R. M., deGouw, J. A.,  
779 Dube, W. P., Field, R. A., Flynn, J. H., Gilman, J. B., Graus, M., Helmig, D., Koss, A.,  
780 Langford, A. O., Lefer, B. L., Lerner, B. M., Li, R., Li, S. M., McKeen, S. A., Murphy,  
781 S. M., Parrish, D. D., Senff, C. J., Soltis, J., Stutz, J., Sweeney, C., Thompson, C. R.,  
782 Trainer, M. K., Tsai, C., Veres, P. R., Washenfelder, R. A., Warneke, C., Wild, R. J.,  
783 Young, C. J., Yuan, B., and Zamora, R.: High winter ozone pollution from carbonyl  
784 photolysis in an oil and gas basin, *Nature*, 514, 351-354, 10.1038/nature13767, 2014.

785 Fernandez, P., Grifoll, M., Solanas, A. M., Bayona, J. M., and Albaiges, J.: Bioassay-  
786 directed chemical analysis of genotoxic components in coastal sediments,  
787 *Environmental Science & Technology*, 26, 817-829, 10.1021/es00028a024, 1992.

788 Fountoukis, C., and Nenes, A.: ISORROPIA II: a computationally efficient  
789 thermodynamic equilibrium model for  $K^+$   $Ca^{2+}$   $Mg^{2+}$   $NH_4^+$   $Na^+$   $SO_4^{2-}$   $NO_3^-$   $Cl^-$   
790  $H_2O$  aerosols, *Atmos. Chem. Phys.*, 7, 4639-4659, 10.5194/acp-7-4639-2007, 2007.  
791 Gilman, J. B., Lerner, B. M., Kuster, W. C., and de Gouw, J. A.: Source signature of  
792 volatile organic compounds from oil and natural gas operations in northeastern  
793 Colorado, *Environ Sci Technol*, 47, 1297-1305, 10.1021/es304119a, 2013.  
794 Harrison, M. A. J., Barra, S., Borghesi, D., Vione, D., Arsene, C., and Iulian Olariu, R.:  
795 Nitrated phenols in the atmosphere: a review, *Atmospheric Environment*, 39, 231-248,  
796 <http://dx.doi.org/10.1016/j.atmosenv.2004.09.044>, 2005a.  
797 Harrison, M. A. J., Heal, M. R., and Cape, J. N.: Evaluation of the pathways of  
798 tropospheric nitrophenol formation from benzene and phenol using a multiphase  
799 model, *Atmos. Chem. Phys.*, 5, 1679-1695, 10.5194/acp-5-1679-2005, 2005b.  
800 Heal, M. R., Harrison, M. A. J., and Neil Cape, J.: Aqueous-phase nitration of phenol by  
801  $N_2O_5$  and  $ClNO_2$ , *Atmospheric Environment*, 41, 3515-3520,  
802 <http://dx.doi.org/10.1016/j.atmosenv.2007.02.003>, 2007.  
803 Herterich, R., and Herrmann, R.: Comparing the distribution of nitrated phenols in the  
804 atmosphere of two German hill sites, *Environ Technol*, 11, 961-972,  
805 10.1080/09593339009384948, 1990.  
806 Inomata, S., Tanimoto, H., Fujitani, Y., Sekimoto, K., Sato, K., Fushimi, A., Yamada, H.,  
807 Hori, S., Kumazawa, Y., Shimono, A., and Hikida, T.: On-line measurements of  
808 gaseous nitro-organic compounds in diesel vehicle exhaust by proton-transfer-reaction  
809 mass spectrometry, *Atmospheric Environment*, 73, 195-203,  
810 <http://dx.doi.org/10.1016/j.atmosenv.2013.03.035>, 2013.  
811 Jacob, D. J.: Heterogeneous chemistry and tropospheric ozone, *Atmospheric*  
812 *Environment*, 34, 2131-2159, [http://dx.doi.org/10.1016/S1352-2310\(99\)00462-8](http://dx.doi.org/10.1016/S1352-2310(99)00462-8),  
813 2000.  
814 Jenkin, M. E., Saunders, S. M., Wagner, V., and Pilling, M. J.: Protocol for the  
815 development of the Master Chemical Mechanism, MCM v3 (Part B): tropospheric  
816 degradation of aromatic volatile organic compounds, *Atmos. Chem. Phys.*, 3, 181-193,  
817 10.5194/acp-3-181-2003, 2003.  
818 Jenkin, M. E., Wyche, K. P., Evans, C. J., Carr, T., Monks, P. S., Alfarra, M. R., Barley,  
819 M. H., McFiggans, G. B., Young, J. C., and Rickard, A. R.: Development and chamber  
820 evaluation of the MCM v3.2 degradation scheme for  $\beta$ -caryophyllene, *Atmos. Chem.*  
821 *Phys.*, 12, 5275-5308, 10.5194/acp-12-5275-2012, 2012.  
822 Karl, T. G., Christian, T. J., Yokelson, R. J., Artaxo, P., Hao, W. M., and Guenther, A.:  
823 The Tropical Forest and Fire Emissions Experiment: method evaluation of volatile  
824 organic compound emissions measured by PTR-MS, FTIR, and GC from tropical  
825 biomass burning, *Atmospheric Chemistry and Physics*, 7, 5883-5897, 2007.  
826 Kaser, L., Karl, T., Guenther, A., Graus, M., Schnitzhofer, R., Turnipseed, A., Fischer,  
827 L., Harley, P., Madronich, M., Gochis, D., Keutsch, F. N., and Hansel, A.: Undisturbed  
828 and disturbed above canopy ponderosa pine emissions: PTR-TOF-MS measurements  
829 and MEGAN 2.1 model results, *Atmos. Chem. Phys. Discuss.*, 13, 15333-15375,  
830 10.5194/acpd-13-15333-2013, 2013.  
831 Kitanovski, Z., Grgić, I., Yasmeen, F., Claeys, M., and Čusak, A.: Development of a  
832 liquid chromatographic method based on ultraviolet-visible and electrospray ionization  
833 mass spectrometric detection for the identification of nitrocatechols and related tracers

834 in biomass burning atmospheric organic aerosol, *Rapid Communications in Mass*  
835 *Spectrometry*, 26, 793-804, 10.1002/rcm.6170, 2012.

836 Lauraguais, A., Coeur-Tourneur, C., Cassez, A., Deboudt, K., Fourmentin, M., and  
837 Choël, M.: Atmospheric reactivity of hydroxyl radicals with guaiacol (2-  
838 methoxyphenol), a biomass burning emitted compound: Secondary organic aerosol  
839 formation and gas-phase oxidation products, *Atmospheric Environment*, 86, 155-163,  
840 <http://dx.doi.org/10.1016/j.atmosenv.2013.11.074>, 2014.

841 Lee, B. H., Lopez-Hilfiker, F., Mohr, C., Kurtén, T. C., Worsnop, D., and Thornton, J.  
842 A.: An Iodide-Adduct High-Resolution Time-of-Flight Chemical-Ionization Mass  
843 Spectrometer: Application to Atmospheric Inorganic and Organic Compounds,  
844 *Environmental Science & Technology*, 10.1021/es500362a, 2014.

845 Lin, P., Liu, J., Shilling, J. E., Kathmann, S., Laskin, J., and Laskin, A.: Molecular  
846 Characterization of Brown Carbon (BrC) Chromophores in Secondary Organic Aerosol  
847 Generated From Photo-Oxidation of Toluene, *Phys Chem Chem Phys*,  
848 10.1039/C5CP02563J, 2015.

849 Mohr, C., Lopez-Hilfiker, F. D., Zotter, P., Prévôt, A. S. H., Xu, L., Ng, N. L., Herndon,  
850 S. C., Williams, L. R., Franklin, J. P., Zahniser, M. S., Worsnop, D. R., Knighton, W.  
851 B., Aiken, A. C., Gorkowski, K. J., Dubey, M. K., Allan, J. D., and Thornton, J. A.:  
852 Contribution of Nitrated Phenols to Wood Burning Brown Carbon Light Absorption in  
853 Detling, United Kingdom during Winter Time, *Environmental Science & Technology*,  
854 47, 6316-6324, 10.1021/es400683v, 2013.

855 Morville, S., Scheyer, A., Mirabel, P., and Millet, M.: Spatial and Geographical  
856 Variations of Urban, Suburban and Rural Atmospheric Concentrations of Phenols and  
857 Nitrophenols (7 pp), *Environ Sci Pollut R*, 13, 83-89, 10.1065/espr2005.06.264, 2006.

858 Müller, M., George, C., and D'Anna, B.: Enhanced spectral analysis of C-TOF Aerosol  
859 Mass Spectrometer data: Iterative residual analysis and cumulative peak fitting,  
860 *International Journal of Mass Spectrometry*, 306, 1-8,  
861 <http://dx.doi.org/10.1016/j.ijms.2011.04.007>, 2011.

862 Natangelo, M., Mangiapan, S., Bagnati, R., Benfenati, E., and Fanelli, R.: Increased  
863 concentrations of nitrophenols in leaves from a damaged forestal site, *Chemosphere*,  
864 38, 1495-1503, [http://dx.doi.org/10.1016/S0045-6535\(98\)00370-1](http://dx.doi.org/10.1016/S0045-6535(98)00370-1), 1999.

865 Olariu, R. I., Klotz, B., Barnes, I., Becker, K. H., and Mocanu, R.: FT-IR study of the  
866 ring-retaining products from the reaction of OH radicals with phenol, o-, m-, and p-  
867 cresol, *Atmospheric Environment*, 36, 3685-3697,  
868 [http://dx.doi.org/10.1016/S1352-2310\(02\)00202-9](http://dx.doi.org/10.1016/S1352-2310(02)00202-9), 2002.

869 Pankow, J. F.: An absorption model of the gas/aerosol partitioning involved in the  
870 formation of secondary organic aerosol, *Atmospheric Environment*, 28, 189-193, Doi:  
871 10.1016/1352-2310(94)90094-9, 1994.

872 Platz, J., Nielsen, O. J., Wallington, T. J., Ball, J. C., Hurley, M. D., Straccia, A. M.,  
873 Schneider, W. F., and Sehested, J.: Atmospheric Chemistry of the Phenoxy Radical,  
874 C<sub>6</sub>H<sub>5</sub>O(•): UV Spectrum and Kinetics of Its Reaction with NO, NO<sub>2</sub>, and O<sub>2</sub>, *The*  
875 *Journal of Physical Chemistry A*, 102, 7964-7974, 10.1021/jp982221i, 1998.

876 Rippen, G., Zietz, E., Frank, R., Knacker, T., and Klöpffer, W.: Do airborne nitrophenols  
877 contribute to forest decline?, *Environmental Technology Letters*, 8, 475-482,  
878 10.1080/09593338709384508, 1987.

879 Rubio, M. A., Lissi, E., Herrera, N., Pérez, V., and Fuentes, N.: Phenol and nitrophenols  
880 in the air and dew waters of Santiago de Chile, *Chemosphere*, 86, 1035-1039,  
881 <http://dx.doi.org/10.1016/j.chemosphere.2011.11.046>, 2012.

882 Sander, R.: Compilation of Henry's law constants (version 4.0) for water as solvent,  
883 *Atmospheric Chemistry and Physics*, 15, 4399-4981, 10.5194/acp-15-4399-2015, 2015.

884 Schwarzenbach, R. P., Stierli, R., Folsom, B. R., and Zeyer, J.: Compound properties  
885 relevant for assessing the environmental partitioning of nitrophenols, *Environmental*  
886 *Science & Technology*, 22, 83-92, 10.1021/es00166a009, 1988.

887 Sekimoto, K., Inomata, S., Tanimoto, H., Fushimi, A., Fujitani, Y., Sato, K., and  
888 Yamada, H.: Characterization of nitromethane emission from automotive exhaust,  
889 *Atmospheric Environment*, 81, 523-531, 10.1016/j.atmosenv.2013.09.031, 2013.

890 Stark, H., Yatawelli, R. L. N., Kimmel, J. R., Bertram, T. H., Thornton, J. A., Jimenez, J.  
891 L., and Worsnop, D. R.: Cluster Formation and Ion Chemistry in the High Pressure  
892 Inlet of a Chemical Ionization Mass Spectrometer: Lessons learned from Field and  
893 Laboratory Studies, 22nd International Symposium on Gas Kinetics, June 18-22, 2012,  
894 Boulder, CO, 2012.

895 Stark, H., Yatawelli, R. L. N., Thompson, S. L., Kimmel, J. R., Cubison, M. J., Chhabra,  
896 P. S., Canagaratna, M. R., Jayne, J. T., Worsnop, D. R., and Jimenez, J. L.: Methods to  
897 extract molecular and bulk chemical information from series of complex mass spectra  
898 with limited mass resolution, *International Journal of Mass Spectrometry*,  
899 10.1016/j.ijms.2015.08.011, 2015.

900 Stockwell, C. E., Veres, P. R., Williams, J., and Yokelson, R. J.: Characterization of  
901 biomass burning emissions from cooking fires, peat, crop residue, and other fuels with  
902 high-resolution proton-transfer-reaction time-of-flight mass spectrometry, *Atmos.*  
903 *Chem. Phys.*, 15, 845-865, 10.5194/acp-15-845-2015, 2015.

904 Tremp, J., Mattrel, P., Fingler, S., and Giger, W.: Phenols and nitrophenols as  
905 tropospheric pollutants: Emissions from automobile exhausts and phase transfer in the  
906 atmosphere, *Water Air Soil Pollut*, 68, 113-123, 10.1007/BF00479396, 1993.

907 Veres, P., Roberts, J. M., Warneke, C., Welsh-Bon, D., Zahniser, M., Herndon, S., Fall,  
908 R., and de Gouw, J.: Development of negative-ion proton-transfer chemical-ionization  
909 mass spectrometry (NI-PT-CIMS) for the measurement of gas-phase organic acids in  
910 the atmosphere, *International Journal of Mass Spectrometry*, 274, 48-55, DOI  
911 10.1016/j.ijms.2008.04.032, 2008.

912 Vione, D., Maurino, V., Minero, C., and Pelizzetti, E.: Phenol photolysis upon UV  
913 irradiation of nitrite in aqueous solution I: Effects of oxygen and 2-propanol,  
914 *Chemosphere*, 45, 893-902, [http://dx.doi.org/10.1016/S0045-6535\(01\)00035-2](http://dx.doi.org/10.1016/S0045-6535(01)00035-2),  
915 2001.

916 Vione, D., Maurino, V., Minero, C., and Pelizzetti, E.: Aqueous Atmospheric Chemistry:  
917 Formation of 2,4-Dinitrophenol upon Nitration of 2-Nitrophenol and 4-Nitrophenol in  
918 Solution, *Environmental Science & Technology*, 39, 7921-7931, 10.1021/es050824m,  
919 2005.

920 Vione, D., Maurino, V., Minero, C., Duncianu, M., Olariu, R.-I., Arsene, C., Sarakha, M.,  
921 and Mailhot, G.: Assessing the transformation kinetics of 2- and 4-nitrophenol in the  
922 atmospheric aqueous phase. Implications for the distribution of both nitroisomers in the  
923 atmosphere, *Atmospheric Environment*, 43, 2321-2327,  
924 <http://dx.doi.org/10.1016/j.atmosenv.2009.01.025>, 2009.

925 Warneke, C., Geiger, F., Edwards, P. M., Dube, W., Pétron, G., Kofler, J., Zahn, A.,  
926 Brown, S. S., Graus, M., Gilman, J., Lerner, B., Peischl, J., Ryerson, T. B., de Gouw, J.  
927 A., and Roberts, J. M.: Volatile organic compound emissions from the oil and natural  
928 gas industry in the Uinta Basin, Utah: point sources compared to ambient air  
929 composition, *Atmos. Chem. Phys.*, 14, 10977-10988, 10.5194/acpd-14-11895-2014,  
930 2014.

931 Warneke, C., Veres, P. R., Murphy, S. M., Soltis, J., Field, R. A., Graus, M. G., Koss, A.,  
932 Li, S. M., Li, R., Yuan, B., Roberts, J. M., and de Gouw, J. A.: PTR-QMS vs. PTR-  
933 TOF comparison in a region with oil and natural gas extraction industry in the Uintah  
934 Basin in 2013, *Atmos. Meas. Tech.*, 8, 411-420, 10.5194/amtd-7-6565-2014, 2015.

935 Wild, R. J., Edwards, P. M., Dube, W. P., Baumann, K., Edgerton, E. S., Quinn, P. K.,  
936 Roberts, J. M., Rollins, A. W., Veres, P. R., Warneke, C., Williams, E. J., Yuan, B.,  
937 and Brown, S. S.: A Measurement of Total Reactive Nitrogen, NO<sub>y</sub>, together with  
938 NO<sub>2</sub>, NO, and O<sub>3</sub> via Cavity Ring-down Spectroscopy, *Environ Sci Technol*, 48,  
939 9609-9615, 10.1021/es501896w, 2014.

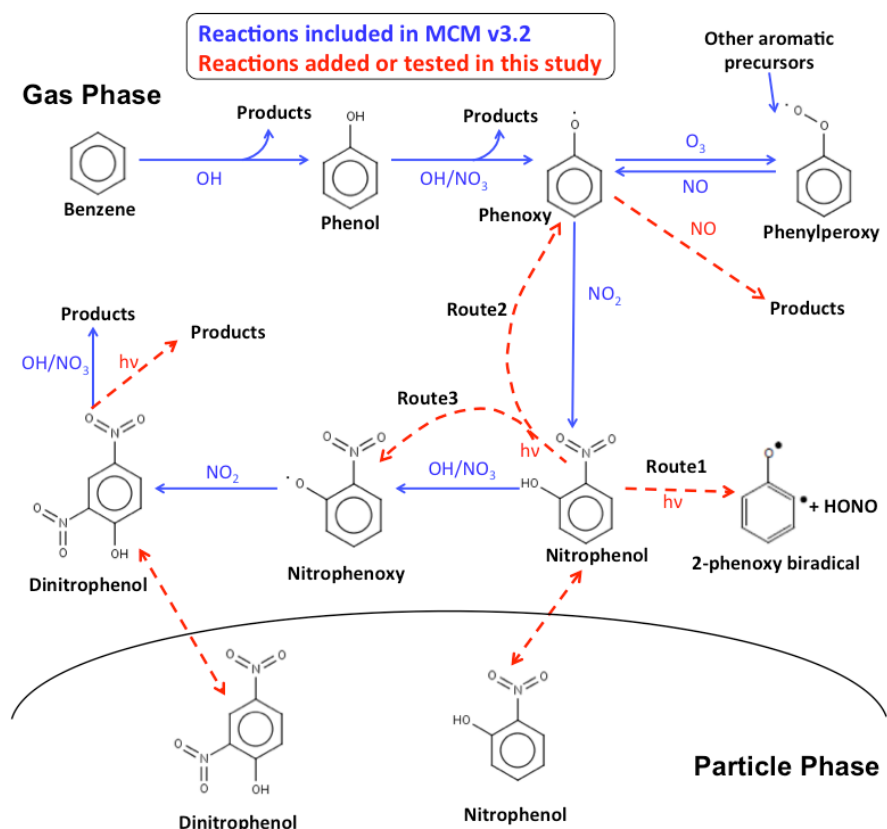
940 Yatawelli, R. L. N., Stark, H., Thompson, S. L., Kimmel, J. R., Cubison, M. J., Day, D.  
941 A., Campuzano-Jost, P., Palm, B. B., Hodzic, A., Thornton, J. A., Jayne, J. T.,  
942 Worsnop, D. R., and Jimenez, J. L.: Semicontinuous measurements of gas-particle  
943 partitioning of organic acids in a ponderosa pine forest using a MOVI-HRToF-CIMS,  
944 *Atmos. Chem. Phys.*, 14, 1527-1546, 10.5194/acp-14-1527-2014, 2014.

945 Yuan, B., Veres, P. R., Warneke, C., Roberts, J. M., Gilman, J. B., Koss, A., Edwards, P.  
946 M., Graus, M., Kuster, W. C., Li, S. M., Wild, R. J., Brown, S. S., Dubé, W. P., Lerner,  
947 B. M., Williams, E. J., Johnson, J. E., Quinn, P. K., Bates, T. S., Lefer, B., Hayes, P. L.,  
948 Jimenez, J. L., Weber, R. J., Zamora, R., Ervens, B., Millet, D. B., Rappenglück, B.,  
949 and de Gouw, J. A.: Investigation of secondary formation of formic acid: urban  
950 environment vs. oil and gas producing region, *Atmos. Chem. Phys.*, 15, 1975-1993,  
951 10.5194/acp-15-1975-2015, 2015.

952 Zhang, X., Lin, Y.-H., Surratt, J. D., and Weber, R. J.: Sources, Composition and  
953 Absorption Ångström Exponent of Light-absorbing Organic Components in Aerosol  
954 Extracts from the Los Angeles Basin, *Environmental Science & Technology*, 47, 3685-  
955 3693, 10.1021/es305047b, 2013.

956

957



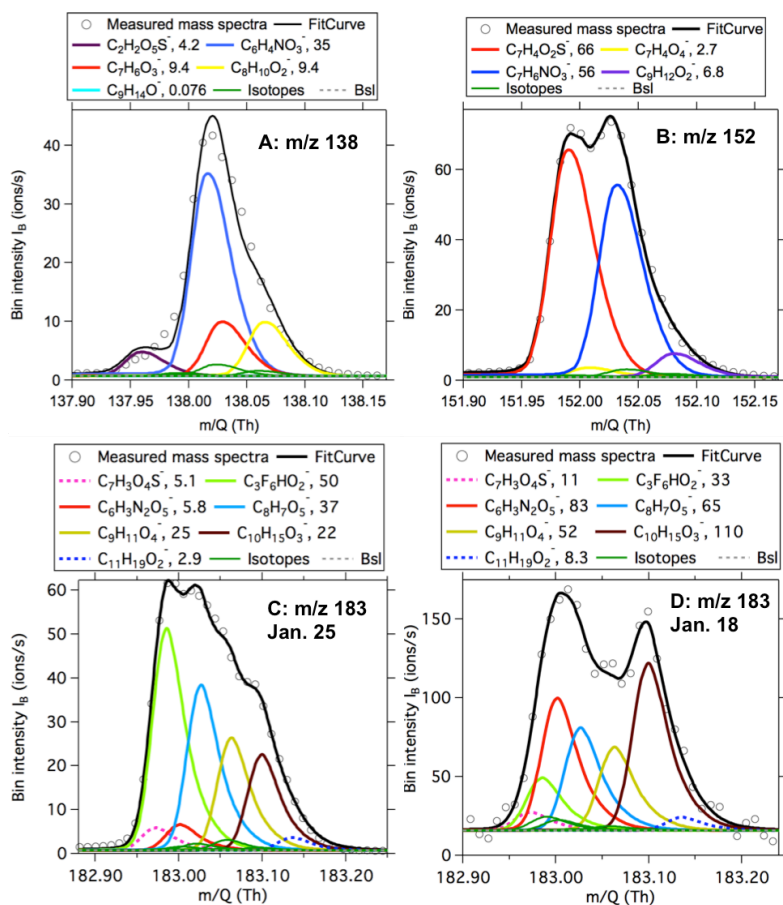
959

960 Figure 1. Formation of phenol, nitrophenol (NP) and dinitrophenol (DNP) from the  
 961 photo-oxidation of benzene in the atmosphere (Jenkin et al., 2003). Reactions in blue are  
 962 included in the MCM v3.2, whereas reactions in red are added or evaluated in this study.  
 963 For NP, DNP and the intermediate radicals, other isomers are expected but not shown for  
 964 the sake of clarity.

965

966

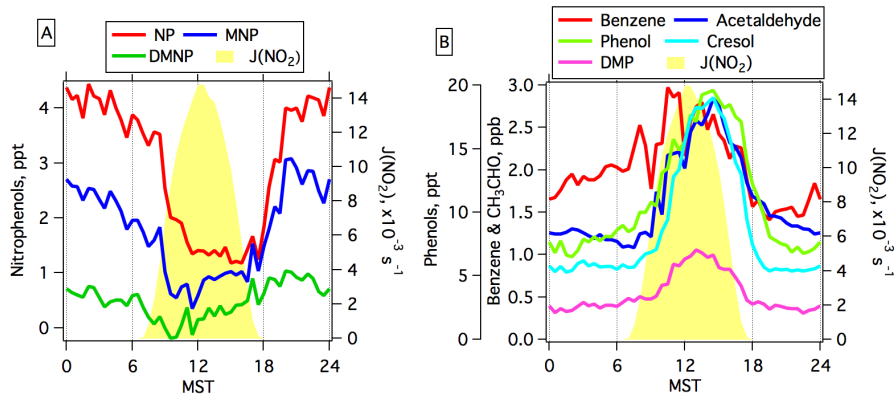




967  
 968  
 969  
 970  
 971  
 972

Figure 2. High-resolution peak fitting to the averaged mass spectra of acetate ToF-CIMS for m/z 138 (A), m/z 152 (B) and m/z 183 (C) on January 25, 2014 and m/z 183 (D) on Jan. 18, 2014 during UBWOS 2014. The dark green lines indicate the calculated isotope signals from lower masses.

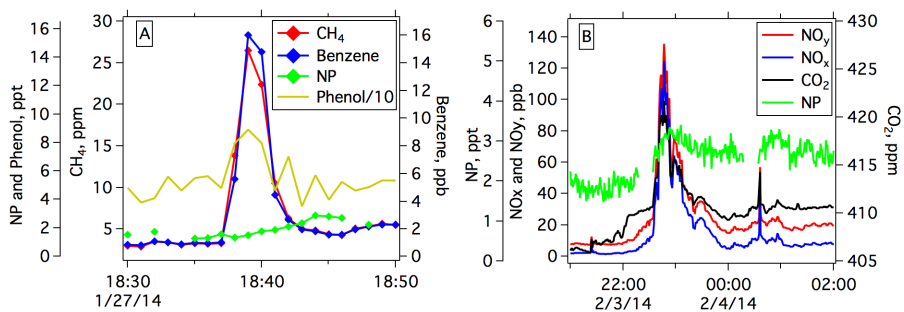




973  
 974 | Figure 3. (A) Diurnal profiles of measured NP, MNP, DMNP. (B) Diurnal profiles of  
 975 benzene, acetaldehyde, phenol, cresol and DMP. Photolysis frequencies of NO<sub>2</sub> are  
 976 shown in both A and B for reference.  
 977

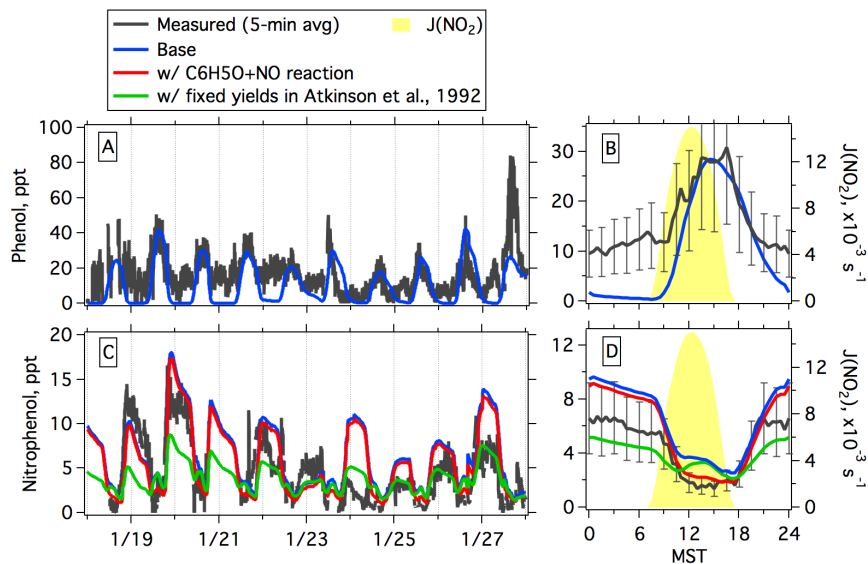
Bin Yuan 12/27/2015 3:45 PM

Deleted: 2



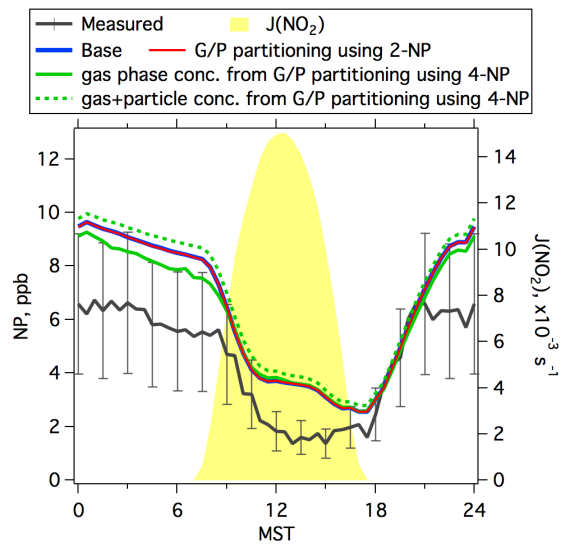
979  
 980 | Figure 4. (A) An episode with high concentrations of methane and benzene on January  
 981 27, 2014 during UBWOS 2014. The source for this episode was fugitive emissions from  
 982 oil and gas activities. (B) An episode with high concentrations of NO<sub>y</sub> and CO<sub>2</sub> on  
 983 February 3, 2014 during UBWOS 2014. The source for this episode was fuel combustion  
 984 (e.g., vehicle exhaust and/or other combustion sources for oil and gas extraction).

Bin Yuan 12/27/2015 3:45 PM  
 Deleted: 3



986  
 987 | Figure 5. (A and C) Comparison of measured and modeled time series of phenol (A) and  
 988 NP (C). (B and D) Diurnal profiles of measured and modeled concentrations of phenol  
 989 (B) and NP (D). Photolysis frequencies of  $\text{NO}_2$  are shown in B and D for reference. Error  
 990 bars in (B) and (D) indicate the accuracies of concentrations of phenol (50%) and NP  
 991 (40%), respectively.  
 992

Bin Yuan 12/27/2015 3:45 PM  
 Deleted: 4



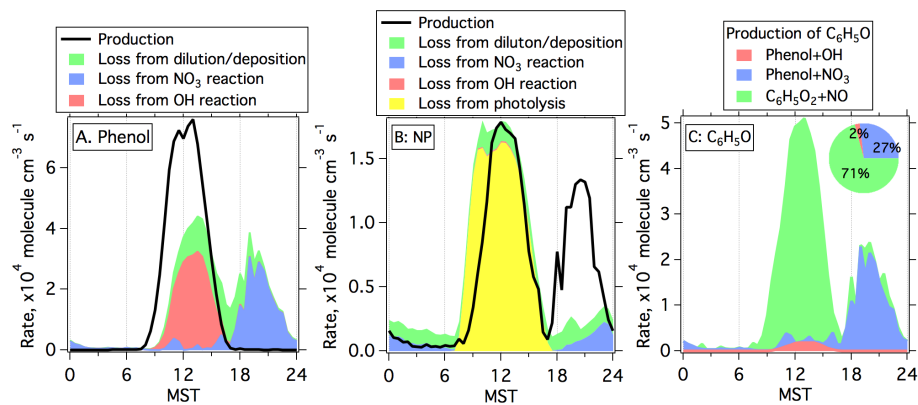
994  
 995 Figure 6. Diurnal profiles of measured and modeled concentrations of NP from the base  
 996 simulation and the simulations considering gas/particle partitioning. Photolysis  
 997 frequencies of NO<sub>2</sub> are shown for reference. Error bars indicate the accuracies of  
 998 concentrations of NP (40%).  
 999

Bin Yuan 12/27/2015 3:45 PM

Deleted: 5

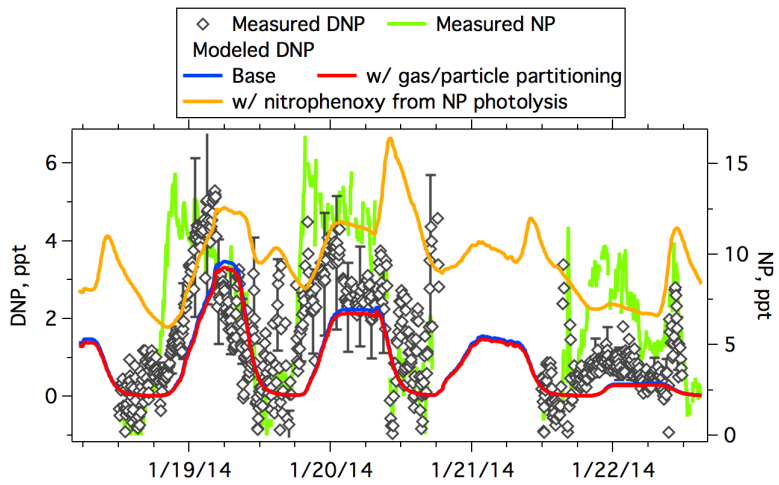
Bin Yuan 12/24/2015 1:58 PM

Deleted: in B and D



1002  
 1003 | Figure 7. Diurnal profiles of production and loss rates from different pathways for phenol  
 1004 (A) and NP (B) derived from the base simulation of the box model. (C) Diurnal profiles  
 1005 of production rates from different pathways for C<sub>6</sub>H<sub>5</sub>O radicals. The inserted pie in C  
 1006 shows contributions from three different pathways to the formation of C<sub>6</sub>H<sub>5</sub>O radicals on  
 1007 a daily basis.  
 1008

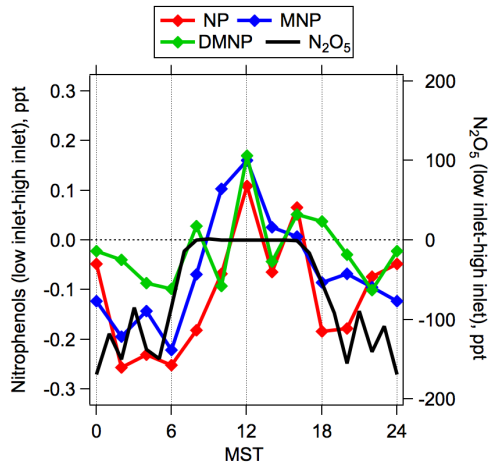
Bin Yuan 12/27/2015 3:45 PM  
 Deleted: 6



1010  
 1011 | Figure 8. Comparison of measured and modeled time series of DNP. Measured time  
 1012 series of NP is also shown for comparison. Error bars indicate the accuracies of DNP  
 1013 concentrations (50%).

1014  
 1015

Bin Yuan 12/27/2015 3:45 PM  
 Deleted: 7



1017  
 1018 | Figure 9. Diurnal profiles of vertical gradients for nitrated phenols measured in January  
 1019 22 – February 1. The measured vertical gradient of N<sub>2</sub>O<sub>5</sub> measured in February 6- 14 is  
 1020 also shown for comparison.  
 1021

Bin Yuan 12/27/2015 3:46 PM  
 Deleted: 8  
 Bin Yuan 12/27/2015 3:46 PM  
 Deleted:

1024 **Tables**1025 Table 1. Sensitivities and detection limits of nitrated phenols in acetate ToF-CIMS.

Species	Abbreviation	Ion	m/z	Sensitivity, ncps/ppt	Ratio to Formic acid <sup>f</sup>	Detection Limit, ppt <sup>f</sup>	
						Method 1	Method 2
Nitrophenol	NP	C <sub>6</sub> H <sub>4</sub> NO <sub>3</sub> <sup>-</sup>	138.0197	13.2 <sup>a</sup>	2.6	0.18	0.45
Methylnitrophenol	MNP	C <sub>7</sub> H <sub>6</sub> NO <sub>3</sub> <sup>-</sup>	152.0353	16.6 <sup>b</sup>	3.3	0.24	0.36
Dimethylnitrophenol + ethylnitrophenol	DMNP	C <sub>8</sub> H <sub>8</sub> NO <sub>3</sub> <sup>-</sup>	166.0510	16.6 <sup>c</sup>	3.3	0.14	0.36
Dinitrophenol	DNP	C <sub>6</sub> H <sub>3</sub> N <sub>2</sub> O <sub>5</sub> <sup>-</sup>	183.0047	10.3 <sup>d</sup>	2.0	0.23	0.58

1026 a: Average from calibrations of 2-NP (8.4 ncps/ppt) and 4-NP (18.0 ncps/ppt).

1027 b: Calibration of 2-methyl-4-nitrophenol.

1028 c: Using the same value as MNP.

1029 d: Calibration using 2,5-dinitrophenol.

1030 e: Based on the determined sensitivity of formic acid at 5.0 ncps/ppt during UBWOS 2014.

1031 f: Method 1 is based on the random errors of observed counts follow Poisson distribution,

1032 whereas method 2 is calculated as the concentrations with counts at three times of standard

1033 deviations of measured background counts (see discussions in text and in Bertram et al. (2011)).

1034

1035

1036

1037

1038

1039

1040 Table 2. Vapor pressure, enthalpy of evaporation ( $\Delta H_{vap}$ ) and calculated concentration1041 fractions in particle phase ( $F_p$ ) for several nitrated phenols

Species	Vapor pressure at 298 K, Torr <sup>a</sup>	$\Delta H_{vap}$ , kJ/mol <sup>a</sup>	$F_p$
2-NP	0.20	53.1	$1.1 \pm 0.9 \times 10^{-4}$
4-NP	$1.4 \times 10^{-3}$	80.0	$5.3 \pm 4.8 \times 10^{-2}$
2,4-DNP	$8.4 \times 10^{-3}$	70.4	$4.6 \pm 4.4 \times 10^{-3}$
2,5-DNP	$1.2 \times 10^{-3}$	68.5	$2.8 \pm 2.7 \times 10^{-3}$

1042 a: Calculated from data in Schwarzenbach et al. (1988).

Bin Yuan 12/30/2015 1:29 PM

**Deleted:** Calibration

Bin Yuan 12/30/2015 1:29 PM

**Deleted:** of

Bin Yuan 12/30/2015 1:29 PM

**Deleted:** to nitrated phenols

Bin Yuan 12/27/2015 4:43 PM

**Deleted:** ppt<sup>f</sup>

Bin Yuan 12/27/2015 4:43 PM

**Deleted:** e



Measurements of DNP using the acetate CIMS were challenging during UBWOS 2014, due to the influence of a fluorine ion ( $\text{C}_3\text{F}_6\text{HO}_2^-$ ,  $m/z$  182.9886) released from the heated Teflon inlet (see Figure S2 for peak fitting example). The release of  $\text{C}_3\text{F}_6\text{HO}_2^-$  ion was supported by much higher signals of this ion from the long-heated inlet compared to the short-unheated inlet, when inlet-switching experiments were conducted in February 2-5 (Figure S1). We also observed that several other fluorine ions were released from the heated inlet ions, such as  $\text{C}_2\text{F}_3\text{O}_2^-$ ,  $\text{C}_3\text{F}_4\text{O}_2^-$  and  $\text{C}_3\text{F}_5\text{O}_2^-$ . The presence of  $\text{C}_3\text{F}_6\text{HO}_2^-$  ion made it difficult to get accurate signals of the ion for of DNP ( $m/z$  183.0047) for most of the time during UBWOS 2014, when the long-heated inlet was used (Figure S1). As a result, we will only use measured DNP data in the beginning of the campaign (January 18-22), when the long heated inlet was not connected to the acetate CIMS and no inlet switching was performed.